AGU PUBLICATIONS

JGR

Journal of Geophysical Research: Atmospheres

RESEARCH ARTICLE
10.1002/2013JD021215

Key Points:
- Seasonal and year-to-year variations in tropospheric ozone over Hyderabad
- Comparison of aircraft vertical profiles of ozone with CCM simulations
- Impact of El Nino and La Nina on profiles of ozone over Hyderabad, India

Correspondence to:
L. K. Sahu,
lokesh@prl.res.in;
l_okesh@yahoo.com

Citation:
Sahu, L. K., V. Sheel, M. Kajino, M. Deushi, S. S. Gunthe, P. R. Sinha, B. Sauvage, V. Thouret, and H. G. Smit (2014), Seasonal and interannual variability of tropospheric ozone over an urban site in India: A study based on MOZAIC and CCM vertical profiles over Hyderabad, *J. Geophys. Res. Atmos.*, *119*, 3615–3641, doi:10.1002/2013JD021215.

Received 19 NOV 2013
Accepted 6 MAR 2014
Accepted article online 12 MAR 2014
Published online 28 MAR 2014

Seasonal and interannual variability of tropospheric ozone over an urban site in India: A study based on MOZAIC and CCM vertical profiles over Hyderabad

L. K. Sahu[1], Varun Sheel[1], M. Kajino[2], M. Deushi[2], Sachin S. Gunthe[3], P. R. Sinha[4], B. Sauvage[5], Valérie Thouret[5], and Herman G. Smit[6]

[1]Physical Research Laboratory, Ahmedabad, India, [2]Meteorological Research Institute, Japan Meteorological Agency, Tsukuba, Japan, [3]Environmental and Water Resources Engineering Division, Department of Civil Engineering, Indian Institute of Technology Madras, Chennai, India, [4]National Balloon Facility, Tata Institute of Fundamental Research, Hyderabad, India, [5]Laboratoire d'Aérologie, CNRS, Observatoire Midi-Pyrénées, UMR 5560, Toulouse, France, [6]Institut für Chemie und Dynamik der Geosphäre, Troposphäre (ICG-2), Forschungszentrum Jülich, Jülich, Germany

Abstract This study is based on the analysis of Measurement of Ozone and Water Vapor by Airbus In-Service Aircraft (MOZAIC) data measured over Hyderabad, India during the years 2006–2008. Tropospheric profiles of O_3 show clear seasonality with high and low values during the premonsoon and monsoon seasons, respectively. Analysis of back trajectory and fire count data indicates major roles for long-range transport and biomass burning in the seasonal variation of O_3. Typically, lower levels of O_3 in the monsoon season were due to the flow of marine air and negligible regional biomass burning, while higher levels in other seasons were due to transport of continental air. In the upper troposphere, relatively low levels of O_3 during the monsoon and postmonsoon seasons were associated with deep convection. In the free troposphere, levels of O_3 also show year-to-year variability as the values in the premonsoon of 2006 were higher by about 30 ppbv compared to 2008. The year-to-year variations were mainly due to transition from El Niño (2006) to La Niña (2008). The higher and lower levels of O_3 were associated with strong and weak wind shears, respectively. Typically, vertical variations of O_3 were anticorrelated with the lapse rate profile. The lower O_3 levels were observed in the stable layers, but higher values in the midtroposphere were caused by long-range transport. In the PBL region, the mixing ratio of O_3 shows strong dependencies on meteorological parameters. The Chemistry Climate Model (CCM2) reasonably reproduced the observed profiles of O_3 except for the premonsoon season.

1. Introduction

The photochemistry of the tropical troposphere largely determines the oxidation capacity of the global atmosphere [*Sauvage et al*., 2007a]. Tropospheric ozone (O_3) is an important greenhouse gas (GHG) because of strong absorption of infrared (IR) radiation at 9.6 μm and hence plays a key role in climate change [*Forster and Shine*, 1997; *Gauss et al*., 2003]. The global radiative forcing contribution of tropospheric O_3 is estimated to be about +0.40 W m^{-2} [*Intergovernmental Panel on Climate Change*, 2013]. In the tropical troposphere, higher levels of solar radiation flux and humidity favor the enhanced formation of the hydroxyl (OH) radical through the photolysis of O_3. Ozone is photodissociated by solar radiation (< 340 nm) to produce an electronically excited O (^1D) atom, which reacts with water vapor (H_2O) and forms OH. Enhanced O_3 near the surface is a serious air pollutant affecting the respiratory health, reducing crop yields, and damaging natural ecosystems [*Emberson et al*., 2003; *Wang and Mauzerall*, 2004]. In India, according to the 2011 census, about 68.4% and 31.16% of the total population (1.21 billion) live in rural and urban regions, respectively. Ozone concentrations in the troposphere have increased significantly since preindustrial times as a direct result of increasing anthropogenic emissions of precursor gases [*Stevenson et al*., 2006]. Observations from the late nineteenth and early twentieth centuries combined with model estimates suggest an increase in tropospheric O_3 from a global mean of 25 Dobson unit (DU) in the preindustrial era to a present value of 34 DU [*Prather et al*., 2001]. In the tropical troposphere, O_3 production is limited by nitrogen oxides ($NOx = NO + NO_2$). In the tropics, the major emissions of NOx are from the activities of biomass burning, biogenic sources, fossil fuel combustion, and lightning [*Sauvage et al*., 2007b; *Monks et al*., 2009]. A variety of anthropogenic activities like combustion of

bio- and fossil- fuels and biomass burning contribute to the emissions of carbon monoxide (CO), methane (CH_4), NOx, and volatile organic compounds (VOCs) in Asia [*Cooper et al.*, 2010; *Lamarque et al.*, 2010; *Sahu*, 2012]. The increasing emission trends of various precursors of O_3 are due to fast industrialization, urbanization, and population growth [*Streets et al.*, 2003a; *Ohara et al.*, 2007]. The regional inventories of various precursor gases in Asia are reported in the several studies [e.g., *Olivier et al.*, 2002; *Heald et al.*, 2003]and bottom-up inventories of NOx indicate an increase of about 44% in south and East Asia during 2001–2006 [*Cooper et al.*, 2010].

India is the second largest energy consumer in Asia and contributes to the emissions of various air pollutants [*Akimoto*, 2003]. Rapid industrialization, urbanization, and traffic growth over the past two decades are responsible for the increasing emission trends of various gaseous pollutants in India. The major sources of O_3 precursors are vehicular transport and biofuel burning, while power generation and industrial emissions contribute to the remaining fraction. Total NOx emission of about 1.9 TgN yr^{-1} for India in the year 2005 was estimated using the satellite-constrained inverse technique [*Ghude et al.*, 2013]. This emission estimate of NOx agrees within 25% with EDGARv4.1 and the INTEX-B estimates. In general, emission estimates of gaseous pollutants are highly uncertain for India mainly due to lack of information on specific sources and accurate statistics. A major uncertainty in tropical photochemistry related to tropospheric O_3 is the quantification of NOx emissions [*Kunhikrishnan et al.*, 2006]. In fact, atmospheric chemistry is complex over India due to a geography encompassing different climatic zones and coemissions from a variety of sources.

Emissions of O_3 precursors from vehicular and industrial sources are expected to show less seasonal variability with slightly higher and lower values during winter and monsoon seasons, respectively. In the case of biomass burning sources, however, the location and timing of emission can be different than those for fossil fuel based emissions [*Streets et al.*, 2003b]. The biomass burning activities in South Asia exhibit strong seasonality with a peak during February–April [*van der Werf et al.*, 2006, 2010]. Long-range transport of O_3 and its various precursors from the different regions of India has been observed to impact the remote marine regions of the Bay of Bengal, Arabian Sea, and Indian Ocean [*Lelieveld et al.*, 2001; *Sahu et al.*, 2006; *Lal et al.*, 2007; *Lawrence and Lelieveld*, 2010]. Transport of South Asian pollutants to the Mediterranean region has been linked to the strong convection during the summer monsoon season [*Park et al.*, 2007]. Vertical measurements of O_3 over several tropical stations in Asia have been reported under the Southern Hemisphere Additional Ozonesondes program [*Thompson et al.*, 2003]. In India, the measurements of O_3 are limited to study the surface variation of O_3 at several locations [*Kumar et al.*, 2012, and references therein]. On the other hand, the vertical measurements of tropospheric O_3 using balloon-borne ozonesondes have been reported for a few locations in India and surrounding marine regions [e.g., *Mandal et al.*, 1999; *Zachariasse et al.*, 2000; *Peshin et al.*, 2001; *Srivastava et al.*, 2011; *Lal et al.*, 2013]. The Measurement of Ozone and Water Vapor by Airbus In-Service Aircraft (MOZAIC) data over Delhi and Chennai have been used to investigate the seasonal and interannual variations of O_3 and H_2O over metro cities of Delhi and Chennai in India [*Sahu et al.*, 2009a, 2010].

In the global troposphere, the major factors that determine the vertical distributions of O_3 include a variety of photochemical and dynamical processes in the atmosphere. Photochemical production in the tropical region is a large contributor to the global budget of O_3 in the troposphere. Tropical dynamics vary on many spatial and temporal scales leading to large variability in tropospheric O_3 [*Cooper et al.*, 2013]. Processes like deep convective outflow, advection, shallow convection, stratosphere troposphere exchange (STE), convective downdraft, convective overshooting, Kelvin waves, etc. play important roles in the distribution of O_3 [*Sherwood and Dessler*, 2003; *Folkins et al.*, 2002]. In other words, vertical distributions of O_3 reflect the interplay of various competing processes in the atmosphere. In the tropics, deep convection is an important force, which can redistribute the profile of O_3 and other trace constituents from the surface to the upper troposphere in a short time scale. Several studies have highlighted the suitability of tropospheric O_3 as a tracer of deep convection [*Paulik and Birner*, 2012, and references therein]. Typically, the lifetime of O_3 varies from 2 to 5 days in the tropical marine boundary layer (MBL) to approximately 90 days in the free troposphere [*Fishman et al.*, 1991; *Lawrence et al.*, 2003]. The impact of anthropogenic and biomass burning in South and Southeast Asia (S-SE Asia) on the tropospheric distribution of O_3 over different regions of the globe have been studied using satellite and model data [*Thompson et al.*, 2001; *Zhang et al.*, 2011]. The vertical distributions of O_3 over Indonesia, Malaysia, and Hong Kong have shown the major impact of biomass burning [*Chan et al.*, 2003; *Yonemura et al.*, 2002; *Thompson et al.*, 2003].

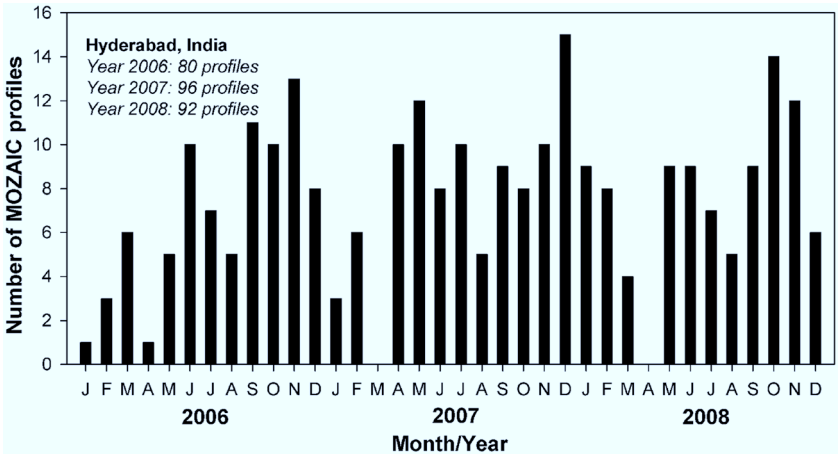

Figure 1. Monthly histogram of the number of MOZAIC profiles measured over Hyderabad during 2006–2008.

The tropical tropospheric O_3 column measured by the Global Ozone Monitoring Experiment [*Burrows et al.*, 1999], Ozone Monitoring Instrument [*Levelt et al.*, 2006], and Microwave Limb Sounder (MLS) instruments [*Waters et al.*, 2006] have been used to study synoptic-scale features. The characteristics of seasonal and interannual variations of vertical O_3 in the tropical troposphere remain unresolved because of the lack of long-term profile observations. The number of O_3-sonde stations in the northern tropics is limited [*Logan*, 1999; *Oltmans et al.*, 2006]. The present manuscript is based on the MOZAIC profiles of tropospheric O_3 and meteorological parameters measured over Hyderabad Airport (17.24°N, 78.43°E) during the years 2006–2008. The primary objective of this study is to investigate the variability of tropospheric O_3 and roles of different atmospheric processes. We have also used satellite fire count and back trajectory model data to investigate the seasonal and interannual variations. A comparison between the MOZAIC observation and the Meteorological Research Institute-Chemistry Climate Model version 2 (MRI-CCM2) simulation of O_3 has also been presented.

2. Description of MOZAIC Program and CCM2 Model

The MOZAIC project was initiated by European scientists, aircraft manufacturers, and airliners in 1993 to study the variability of the chemical composition in the atmosphere [*Marenco et al.*, 1998]. The flights have been sponsored by Air France, Austrian Airlines, Lufthansa, and Sabena/Air France. Measurements on board Airbus A340s have been operational since August 1994. In the second phase (1997–2000), the measurements of O_3 and H_2O were continued while sensors for CO and of total odd-nitrogen (NOy) were developed for deployment. Measurements of O_3 were performed using a dual beam ultra violet absorption instrument from Thermo-Electron (Model 49-103), which has a detection limit of 2 ppbv. Overall, the upper limit of error in the measurements of O_3 was estimated to be ± (2.0 ppbv + 2%) [*Thouret et al.*, 1998a, 1998b]. The response time of the O_3 analyzer is 4 s, which translates into a vertical resolution of about 30 m of altitude. The detailed description of the sampling procedure, measurement technique, calibration, instrument validation, and quality testing is reported in *Thouret et al.* [1998b]. The MOZAIC measurements of O_3 combined with meteorological data are being used to (1) study the global climatology of O_3 and H_2O in the troposphere [*Thouret et al.*, 1998a; *Helten et al.*, 1999]; (2) understand the vertical and temporal distributions of O_3 and H_2O over various locations of the world [*Sauvage et al.*, 2005]; (3) investigate the seasonal and geographical variations in view of their natural and anthropogenic sources, roles of STE, and horizontal and vertical air circulation [*Cooper et al.*, 2006]; and (4) validate chemical transport models [*Marenco et al.*, 1998; *Sauvage et al.*, 2007b]. Measurements taken during both take off and landing of the aircraft have been used as vertical profile data. In this study, we have used a total of 268 profiles measured over the Hyderabad Airport during the years 2006–2008. The monthly histogram of the number of the MOZAIC profiles is shown in Figure 1. All the profiles were measured during the nighttime, between 22 and 24 h local time.

The MRI-CCM2 is a global chemistry-climate model that simulates the distribution and evolution of O_3 and other trace gases in the troposphere and the stratosphere [*Deushi and Shibata*, 2011]. The previous version

(MRI-CCM1) was a stratospheric chemistry-climate model [*Shibata et al*., 2005]. Version 2, however, incorporates an elaborate mechanism for the photochemistry of HOx-NOx-CH_4-CO, degradation of nonmethane hydrocarbons, and heterogeneous reactions on tropospheric aerosols, so it can simulate tropospheric O_3 chemistry as well as stratospheric chemistry. The chemistry module of the MRI-CCM2 is coupled with an MRI atmospheric general circulation model (MRI-AGCM3) [*Yukimoto et al*., 2011] via a simple and flexible coupler (Scup) [*Yoshimura and Yukimoto*, 2008]. The horizontal coordinate of the MRI-CCM2 is a Gaussian grid with a resolution of about 110 km. In the vertical, a hybrid p-σ coordinate is used with 64 layers extending from the surface to the mesopause (0.01 hPa ≈ 80 km). This model is currently used to predict the distribution of photochemical oxidants near the surface in support of operational air quality forecasts of the Japan Meteorological Agency (JMA). Moreover, it is used to provide time-varying lateral and upper boundary concentrations of gaseous species for a regional air quality model over northeast Asia (RAQM2) [*Kajino et al*., 2012].

We performed a simulation for the period 2005–2008 by using the MRI-CCM2. The initial concentrations of chemical species were not fully stabilized at the beginning of the simulation, so the transient concentrations during the first year of the simulation were discarded and then the stabilized ones during the last 3 years were analyzed. In this simulation, the horizontal wind field was nudged toward the JMA Climate Data Assimilation System (JCDAS) analysis [*Onogi et al*., 2007] by using a Newtonian relaxation technique with an 18 h e-folding time. Trace gas emissions from the burning of fossil fuels by industrial activities and aircraft (anthropogenic sources) and from biomass burning (anthropogenic and natural sources) and from vegetation, soils, and the ocean (natural sources) were prescribed. Anthropogenic emission data were taken from the MACCity data set developed as part of two European Union projects: Monitoring Atmospheric Composition and Climate (MACC) and CityZen [*Granier et al*., 2011; *Lamarque et al*., 2010]. Biomass burning emission data were taken from the Global Fire Emissions Database version 3 (GFED3) [*Van der Werf et al*., 2010]. Biogenic and oceanic emissions were taken from *Horowitz et al*. [2003, and references therein]. Present period global mean concentrations of CO_2, N_2O, CH_4, chlorofluorocarbons, and halons were prescribed at the surface. The emission of NOx from lightning was diagnosed at 6 h intervals in the chemistry module using the meteorological fields from the MRI-AGCM3 [*Deushi and Shibata*, 2011].

3. Site and Local Emission Sources in Hyderabad

Hyderabad is the largest city and capital of Andhra Pradesh, a state in southern India. It lies on the Deccan Plateau, 541 m above the sea level, over an area of approximately 650 km^2. The population of the city was about 6.8 million as of the 2011 census. The Rajiv Gandhi International Airport is located 22 km south of the Hyderabad city centre. The transportation sector is one of the fastest growing in Hyderabad, due to a growing population and an economy linked to the expanding information technology industry. There are over 2.4 million vehicles in Hyderabad as of March 2011 (http://hyderabad.trafficpolice.co.in/). The vehicular traffic in Hyderabad has been increasing at an average of about 11% yr^{-1} since 2001 and comprises two wheelers (74%), motor cars/jeeps (16%), goods vehicles (4%), auto rickshaws (3%), taxis (1.5%), buses (0.6%), and state carriages/minibuses (1%). Emissions from vehicular exhaust make a dominant contribution to air pollutants such as particulate matter, CO, NOx, etc. According to a report (available at http://www.cgrer.uiowa.edu/people/sguttiku/ue/reports), the emission estimates of PM_{10}, SO_2, and NOx were 8410 t yr^{-1}, 6304 t yr^{-1}, and 39,263 t yr^{-1} from vehicular sources in Hyderabad during 2006. The Bharat Stage III (Euro 3) type regulation had been regulated during the study period at Hyderabad. There exists a large industrial sector covering metal and agro processing, paints, tanning, and pharmaceuticals in the outskirts of Hyderabad City. The emissions of these species from industrial sources ranked second largest in contribution. Major industries such as the Electronics Corporation of India Limited, Hindustan Cables Limited, petroleum storage containers, Hindustan Petroleum Corporation Limited, and Bharat Petroleum Corporation Limited are located in the northeast (NE) and northwest (NW) directions of the airport [*Swamy et al*., 2012].

4. General Circulation and Meteorology

Typically, the seasons in India are categorized as winter (December–February), premonsoon (March–May), monsoon (June–September), and postmonsoon (October–November) [*Sinha et al*., 2013]. The large-scale circulation in S-SE Asia is primarily driven by the seasonal movement of the Intertropical Convergence Zone (ITCZ) [*Asnani*, 2005; *Sahu et al*., 2013a]. The monsoon and winter seasons are associated with the northward

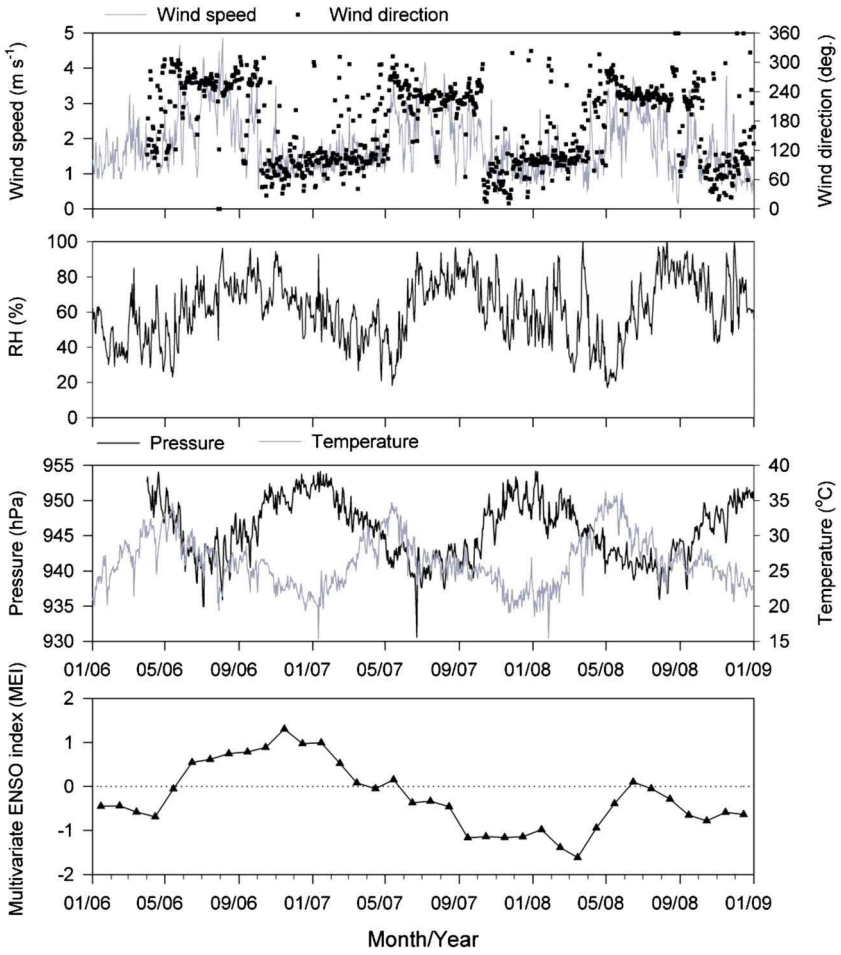

Figure 2. The surface level time series plots of daily meteorological parameters at Hyderabad and monthly ENSO data during 2006–2008.

and southward progression of the ITCZ, respectively. The southwest (SW) winds transport cleaner marine air from the Arabian Sea and the Indian Ocean during the monsoon season. In the winter season, the prevailing winds from the NE and NW directions transport continental pollutants. The climate in Hyderabad is relatively dry during the winter and premonsoon seasons but humid weather with frequent rainfall prevails during the monsoon season. The premonsoon and postmonsoon periods represent the transitions between summer monsoon and winter circulations and are influenced by the mixed air masses from the marine and continental regions. This discussion about the seasonality in the pattern of long-range transport is very typical. However, as discussed in section 6.1, careful analysis of back trajectory data reveals differences in the pattern of long-range transport between El Niño and La Niña years. For example, in the upper troposphere during the postmonsoon season, transport from Africa and South Asia dominated during the El Niño and La Niña years, respectively. Time series of the surface level wind speed, wind direction, relative humidity (RH), pressure, and temperature from January 2006 to December 2008 are shown in Figure 2. The meteorological data were recorded at the national balloon facility of the Tata Institute of Fundamental Research located at about 15 km from the city center of Hyderabad in the NE direction. All the meteorological parameters show significant day-to-day and seasonal variations. The monthly mean temperature varied from a minimum of 21°C in the month of December to a maximum of 32°C in April–May. The monthly mean wind speed varied in the range of 2.0–4.5 m s^{-1} in the monsoon season, however, rather calm weather conditions (1.0–1.5 m s^{-1}) prevailed during the winter season. Based on the data presented in Figure 2, the averages of surface level pressure were 940 hPa, 922 hPa, 908 hPa, and 949 hPa during the winter, premonsoon, monsoon, and postmonsoon seasons, respectively. Typically, the monthly RH varied from a minimum of 30% in May to a maximum of 85% in August. The average values of RH were 61%, 48%, 78%, and 68% during the winter,

premonsoon, monsoon, and postmonsoon seasons, respectively. The El Niño–Southern Oscillation (ENSO) is parameterized as the multivariate ENSO Index (MEI) based on different variables like sea level pressure, wind components, sea surface temperatures (SST), air temperatures, and total cloudiness fraction of the sky [*Allan et al*., 1996]. As shown in Figure 2, the times series variation of MEI indicates the transition from El Niño in 2006 to La Niña in 2008.

5. Results

5.1. Seasonal Variation of O_3

The monthly mean vertical curtain plots of the MOZAIC measurements of O_3 (ppbv), H_2O (g kg^{-1}) and wind speed (m s^{-1}) over Hyderabad from January 2006 to December 2008 are shown in Figure 3. The mixing ratio of O_3 shows large vertical variation in the troposphere throughout the period of observations. Nonetheless, a tendency to increase with height can be clearly noticed. For each month, the levels of O_3 in the planetary boundary layer (PBL) region were lower than the free tropospheric values. The low values of O_3 in the PBL could be due to chemical loss by NO titration, and the suppressed boundary layer as MOZAIC profiles were measured during the night [*Lal et al*., 2008; *Reddy et al*., 2011]. The seasonal variation of O_3 at all altitudes over Hyderabad can be clearly noticed. In the PBL region (< 2 km), the mixing ratio of O_3 was measured to be highest in the winter season and lowest in the monsoon season. In this region of the troposphere, the monthly mean mixing ratio of O_3 was highest (54 ± 5 ppbv) in the month of January and lowest (18 ± 2 ppbv) in the month of August. However, the distribution of O_3 in the free troposphere shows a slight shift in the seasonal pattern as the highest and lowest values were observed in the premonsoon and monsoon seasons, respectively. The monthly mean free tropospheric O_3 mixing ratios were highest (66 ± 2 ppbv) in April and lowest (32 ± 3 ppbv) in August. Moderate levels of O_3 were measured during the postmonsoon months throughout the troposphere (below 12 km).

As shown in Figure 3 (middle), the vertical profiles of H_2O concentration also show large month-to-month variation over Hyderabad. The concentrations of H_2O were measured to be highest in the PBL region and decreased rapidly with increasing altitude during all the months of the year. Despite the large altitudinal dependency, the profiles of H_2O show clear seasonality, particularly in the lower and middle troposphere. Overall, the levels of H_2O were measured to be highest in the monsoon season and lowest in the winter season. The seasonal variation of H_2O concentration appears to be opposite in phase to that of the O_3 mixing ratio over Hyderabad. As shown in Figure 3 (bottom), the monthly wind speed increases gradually with increasing height in the troposphere during winter, premonsoon, and postmonsoon seasons. However, the wind speed profiles in the monsoon season show distinct variability. In this season, the wind speed remained high in the lower and upper troposphere but the lowest were measured in the middle troposphere. At least in the middle-upper tropospheric region (6–12 km of altitudes), the seasonality of wind speed is similar to that of O_3 but opposite to that of H_2O to some extent. Typically, the time series of tropospheric O_3 and H_2O are negatively correlated in the tropics [*Ziemke et al*., 2007]. This suggests convective lifting of air transporting low amounts of O_3 and high amounts of H_2O from the boundary layer. Therefore, this out-of-phase seasonal variability over Hyderabad is expected. On the other hand, the relation between the mixing ratio of O_3 and wind speed is subject to the change in wind direction. Typically, strong winds prevailing from the polluted Indo-Gangetic Plain (IGP) and other continental regions can enhance the levels of O_3 while transport from the cleaner marine regions of Bay of Bengal and Arabian Sea can cause substantial reduction [*Lal et al*., 2008; *Swamy et al*., 2012]. In this paper, we have presented a detailed investigation of the relations between O_3 and wind speed by taking account the wind direction.

The seasonal mean MOZAIC vertical profiles of O_3 over Hyderabad based on the combined observations from 2006 to 2008 are shown in Figure 4. The box-whisker plot with 150 m height interval shows the mean, median, and 5th/95th percentiles for each season. In the PBL region, the average mixing ratios of O_3 were 51 ± 14 ppbv, 46 ± 17 ppbv, 24 ± 12 ppbv, and 41 ± 14 ppbv in the winter, premonsoon, monsoon, and postmonsoon seasons, respectively. In the winter season, the vertical profile of O_3 mixing ratio shows layered structure in the troposphere. Near the surface, in a layer between 0.5 km and 2.5 km, the maximum mixing ratio of O_3 was 57 ppbv. In the midtroposphere, between 4 km and 8 km, the enhancement of O_3 was up to 50 ppbv. However, lower values of about 45 ppbv were observed in the layers at 3–4 km and 8–11 km.

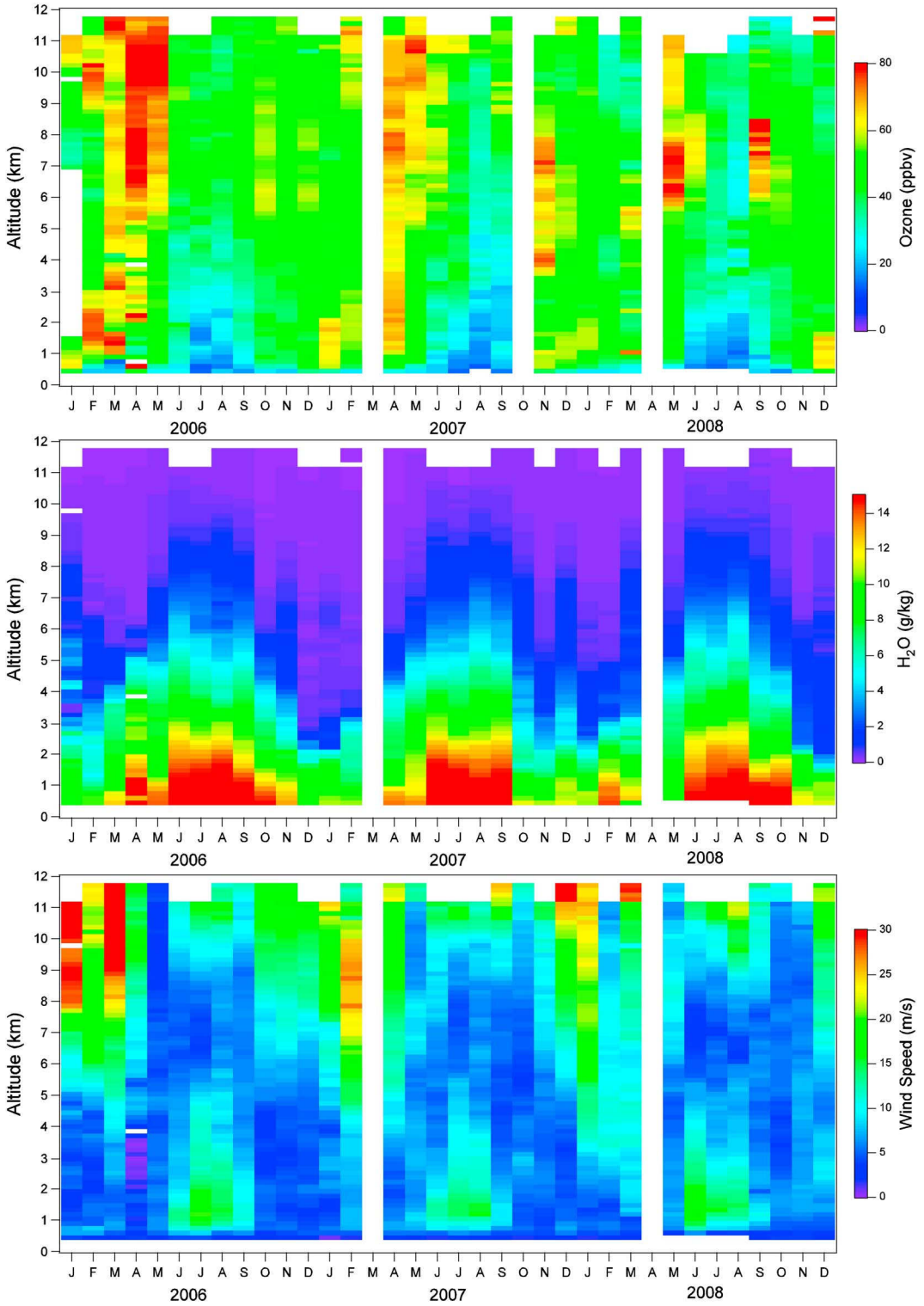

Figure 3. Time versus altitude curtain of monthly means of (top) ozone (O_3), (middle) water vapor (H_2O), and (bottom) wind speed using the MOZAIC data over Hyderabad during 2006–2008.

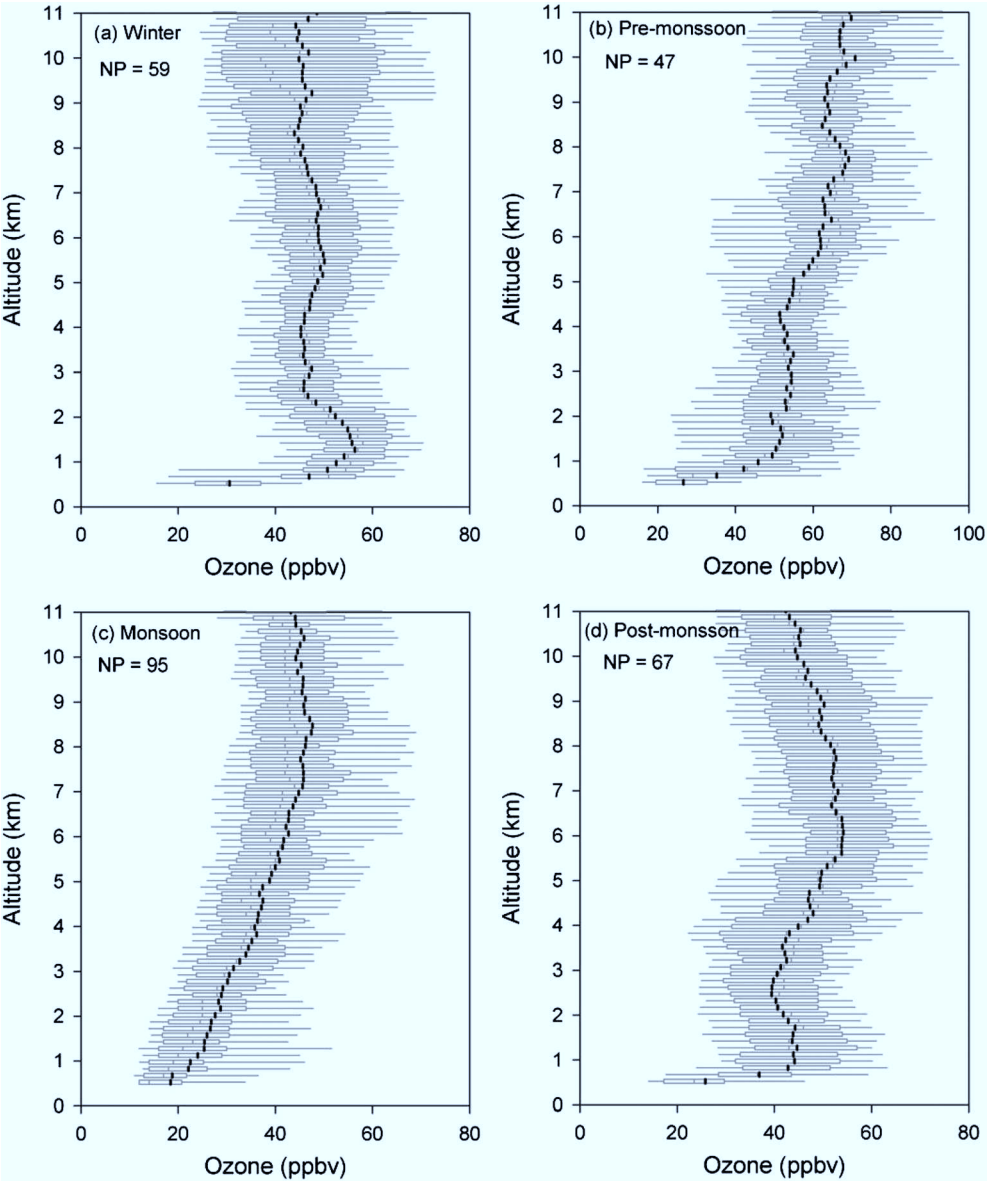

Figure 4. The MOZAIC profiles of O_3 using 150 m height interval data along with the average, 5th percentile, and 95th percentile over Hyderabad during the different seasons of 2006–2008. NP represents number of MOZAIC profiles.

In the premonsoon season, the mixing ratio of O_3 shows a stepwise increase with the altitude. In this season, the mixing ratio of O_3 increased rapidly from 25 ppbv near the surface to 52 ppbv at 1.5 km and a broad layer of enhanced O_3 with peak value of ~70 ppbv was observed at 4–8 km. In the monsoon season, the mixing ratio of O_3 increased gradually from the near surface value of 20 ppbv to 37 ppbv at 4 km. However, less prominent compared to other seasons, the enhanced mixing ratio of O_3 with a peak value of 47 ppbv was observed at 4–8 km in the monsoon season. In the postmonsoon season, the mixing ratio of O_3 increased rapidly from 25 ppbv to 45 ppbv in the PBL region. In this season, a broad layer of enhanced O_3 with a peak value of 55 ppbv was observed at 4–8 km. However, except for the premonsoon season, slightly decreasing trends of O_3 with altitude were noticed in the upper troposphere (8–11 km).

The separation between profiles of 5th and 95th percentiles varies with altitude indicating the different ranges of variation in tropospheric O_3. The average ranges of 5th–95th percentiles of O_3 in the PBL region were 30–67 ppbv, 22–67 ppbv, 12–48 ppbv, and 22–61 ppbv during the winter, premonsoon, monsoon,

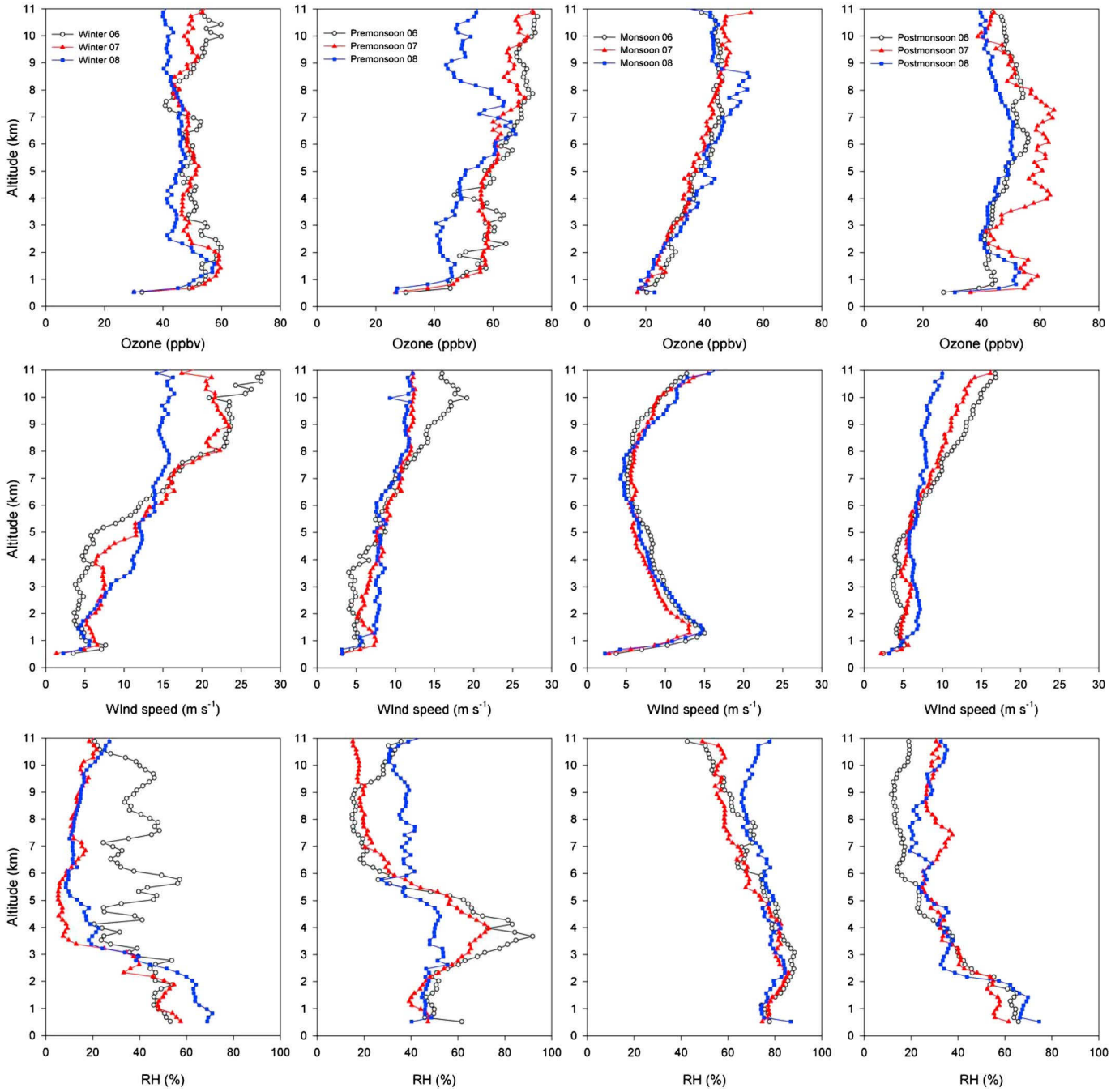

Figure 5. The mean MOZAIC profiles of O_3, wind speed, and relative humidity (RH) over Hyderabad during the different seasons of 2006–2008.

and postmonsoon seasons, respectively. In the upper troposphere, except for the monsoon season, the range of O_3 variability increased with increasing altitude. The profile of the 5th percentile has been assumed as the background profile of O_3 in the troposphere for a given season [*Sahu et al.*, 2009b, 2011]. In the free troposphere, the background mixing ratio of O_3 increased with altitude during the premonsoon and monsoon seasons but decreased during winter and postmonsoon seasons. In section 6.2, we have investigated the role of convective transport in the distribution of O_3 using derived parameters like equivalent potential temperature (EPT or θ_e) and lapse rate (LR).

In Figure 5, the seasonal mean vertical profiles of O_3, wind speed, and RH are plotted for each year separately. In the PBL region, the enhanced levels of O_3 during winter, premonsoon, and postmonsoon seasons were

Table 1. The Seasonal Means of Ozone, Wind Speed, and RH in the Lower and Upper Free Troposphere During Each Year of 2006–2008 Over Hyderabad

	Ozone (ppbv)			Wind Speed ($m\,s^{-1}$)			RH (%)		
Year	2006	2007	2008	2006	2007	2008	2006	2007	2008
				Altitude (2–4 km)					
Winter	53 ± 4	49 ± 4	44 ± 2	4 ± 1	7 ± 1	9 ± 2	36 ± 10	26 ± 15	35 ± 6
Premonsoon	58 ± 5	57 ± 1	44 ± 3	5 ± 1	7 ± 1	8 ± 1	70 ± 14	62 ± 9	50 ± 3
Monsoon	31 ± 3	30 ± 3	32 ± 4	10 ± 1	9 ± 1	10 ± 2	85 ± 3	82 ± 12	81 ± 2
Postmonsoon	43 ± 1	49 ± 7	42 ± 2	4 ± 1	5 ± 1	7 ± 1	41 ± 7	40 ± 7	37 ± 6
				Altitude (8–11 km)					
Winter	53 ± 4	49 ± 3	42 ± 1	24 ± 2	21 ± 1	15 ± 1	35 ± 8	15 ± 3	18 ± 5
Premonsoon	72 ± 2	68 ± 3	50 ± 4	16 ± 2	12 ± 1	12 ± 1	24 ± 8	18 ± 1	36 ± 3
Monsoon	44 ± 2	48 ± 3	45 ± 5	8 ± 2	9 ± 3	10 ± 3	56 ± 6	56 ± 3	70 ± 4
Postmonsoon	49 ± 3	47 ± 5	42 ± 2	14 ± 2	12 ± 2	8 ± 1	15 ± 3	29 ± 2	29 ± 5

associated with the calm wind but high levels of RH. However, not shown in the figure, the profiles of potential temperature (PT) in the PBL suggest unstable condition as it is almost constant or increases at a slower rate with height. In the well-mixed PBL, the concentration of H_2O and PT are expected to remain nearly constant with altitude. On the other hand, the enhanced mixing ratios of O_3 observed in the middle troposphere (4–8 km) coincide with lower values of both wind speed and RH. In this region of the troposphere, PT increases more rapidly with height in the midtroposphere during all the seasons. This is the region where air masses stop rising because of the static stability of the free troposphere in the tropics. Consistently, the mass flux divergence from clouds is weak within the pseudoadiabatic layer (5–10 km) in the tropical region [*Folkins and Martin*, 2005].

5.2. Interannual Variation of O_3

Analysis of MOZAIC data from 2006 to 2008 also provides an opportunity to investigate the year-to-year variation of tropospheric O_3 over Hyderabad. As shown in Figure 5, the seasonal mean profiles of O_3 and meteorological parameters vary significantly from year to year. While the shape of O_3 profiles remained similar, the levels of O_3 in 2008 were lower compared to those during 2006 and 2007. The major interannual differences can be seen in the profiles for the premonsoon and postmonsoon seasons. In these seasons, the year-to-year differences in O_3 and meteorological parameters were highest in the lower (2–4 km) and upper (8–11 km) troposphere. Except for the postmonsoon season, the interannual differences were lowest in the midtroposphere. The seasonal means of O_3, wind speed, and RH in the lower and upper free troposphere during each year of observations are presented in Table 1. In the upper troposphere, except for the monsoon season, the mean mixing ratios of O_3 were highest and lowest during the years 2006 and 2008, respectively. The year-to-year variation of wind speed shows the opposite trend to that of O_3 in the lower troposphere, but correlated variation was observed in the upper troposphere. In the upper troposphere, the mean values of RH during the premonsoon, monsoon, and postmonsoon seasons of 2006 were lower than those observed during 2008. The year-to-year variation of O_3 and meteorological parameters in the upper troposphere indicate the impact of weaker and stronger deep convection during the years 2006 and 2008, respectively [*Cooper et al.*, 2013].

We have investigated the role of transition from El Niño 2006 to La Niña 2008 conditions in the year-to-year variation of O_3 and several meteorological parameters over Hyderabad. In 2006, the mean wind shears between the lower and upper troposphere were 20 $m\,s^{-1}$, 11 $m\,s^{-1}$, and 10 $m\,s^{-1}$ during the winter, premonsoon, and postmonsoon seasons, respectively (see Table 1). On the other hand, in 2008, the profiles show weaker wind shears of 6 $m\,s^{-1}$, 4 $m\,s^{-1}$, and 1 $m\,s^{-1}$ during the winter, premonsoon, and postmonsoon seasons, respectively. The year-to-year variation in upper tropospheric O_3 is consistent with the variation of wind shear strength over Hyderabad. For example, the enhanced O_3 mixing ratios (72 ± 2 ppbv) were associated with the strong wind shear (11 $m\,s^{-1}$) in the upper troposphere during the premonsoon of year 2006. On the other hand, the lower O_3 mixing ratios (40–50 ppbv) were associated with the weaker wind shears (1–4 $m\,s^{-1}$) in the upper troposphere during the premonsoon and postmonsoon seasons of 2008.

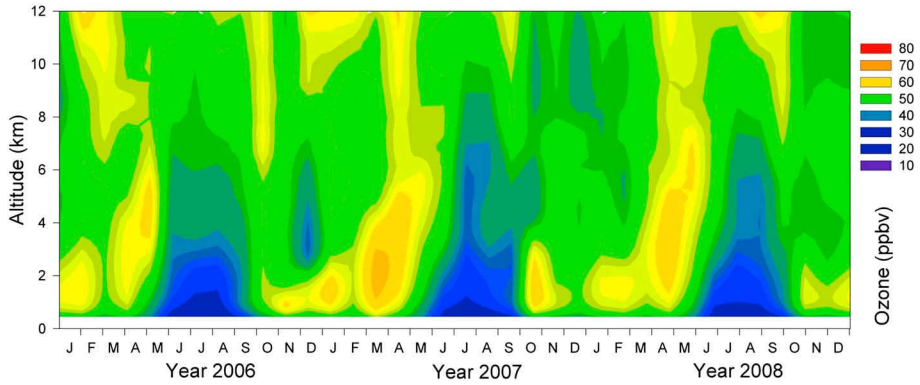

Figure 6. Time series of monthly mean MRI-CCM2 profiles of O_3 over Hyderabad during 2006–2008.

Numerous observational and modeling studies have suggested the presence of tropical cyclones (TC) under very weak vertical shear of horizontal wind between the lower and upper troposphere [e.g., *Wong and Chan*, 2004; *Girishkumar and Ravichandran*, 2012]. During the years 2007–2008, the existence of low-level cyclonic vorticity and enhanced convection provided favorable conditions for TC activity due to the prevailing La Niña condition. The TCs over the Bay of Bengal region occur more frequently in the postmonsoon (primary TC period) and premonsoon (secondary TC period) seasons [*Girishkumar and Ravichandran*, 2012]. In contrast to the La Niña years, the strong vertical wind shears could have inhibited the deep convection during the El Niño year 2006. The outgoing long-wave radiation anomalies over India show suppressed convection during El Niño and deep convection during La Niña regimes [*Bansod*, 2011]. Observations from the satellite and airborne instruments have also shown the decline of tropospheric O_3 over peninsular India during the episodes of tropical storms during November 2006 [*Barret et al.*, 2011]. Therefore, the lower O_3 mixing ratios over Hyderabad were attributed to the uplift and westward transport of cleaner air masses from the marine boundary layer (MBL) of the Bay of Bengal by tropical storms during the La Niña period. Several studies have observed large interannual variability in tropical tropospheric O_3 associated with El Niño and La Niña events [*Ziemke and Chandra*, 2003, and references therein].

5.3. CCM Simulations of O_3

The contour plot of monthly mean CCM2 simulations of tropospheric O_3 over Hyderabad from the years 2006 to 2008 is shown in Figure 6. In the PBL region, the simulations of O_3 show values of 50–60 ppbv in the winter, premonsoon, and postmonsoon seasons but lower values of 20–30 ppbv in the monsoon season. The pattern and strength of seasonality in the PBL region remained almost same as the year-to-year differences are not significant. On the other hand, the pattern and strength of seasonality in the free troposphere show noticeable year-to-year differences. In the free troposphere, the decrease in O_3 from premonsoon to monsoon and then increase in the postmonsoon season of 2006 were rather sharp compared to the gradual transitions simulated for the years 2007 and 2008. For example, between 6 km and 12 km, the enhancements of O_3 up to 50–55 ppbv in the month of October 2006 were about 10–15 ppbv higher than those simulated for the same month of the years 2007 and 2008. In the postmonsoon season of 2006, the significant increase in the levels of O_3 over Hyderabad clearly indicates the impact of extensive biomass burning in Indonesia caused by El Niño conditions. From July to November, the ENSO-induced biomass burning in the islands of Indonesia and Malaysia makes the S-SE Asia region unique in terms of the extreme interannual variability. The strong positive O_3 anomaly of about 30 ppbv detected by the Tropospheric Emission Spectrometer instrument over the Bay of Bengal during October of 2006 confirms the impact of extensive Indonesian fires in 2006 [*Nassar et al.*, 2009]. The Model for Ozone and Related chemical Tracers (MOZART)-4 simulation and MOZAIC data over Bangkok city show strong impact of biomass burning during 2006 [*Sahu et al.*, 2013a, 2013b]. The Microwave Limb Sounder (MLS) observations also showed enhanced levels of upper tropospheric O_3 in the tropical Asian region [*Zhang et al.*, 2011]. In the tropical upper troposphere, the fire-related emissions of O_3 precursors are transported northwestward to S-SE Asia by the western North Pacific subtropical high. For example, the MLS data show widespread enhancements of CO at 215 hpa (~11 km) between 20°S and 20°N of latitudes during 2006 [*Zhang*

et al., 2011]. Enhancements in the mixing ratio of CO were also observed over S-SE Asia during the Indonesian forest fires in 2006 by the Atmospheric Chemistry Fourier Transform Spectrometer and Measurements of Pollution in the Troposphere instruments [*Yurganov et al*., 2008; *Srivastava and Sheel*, 2012]. On the other hand, significant decrease in the levels of O_3 over Hyderabad during the postmonsoon season of 2008 indicates the role of tropical cyclonic conditions caused by La Niña.

5.4. Comparison Between MOZAIC and CCM2 Profiles of O_3

The average profiles of MOZAIC measurements and CCM2 simulations of O_3 for the different seasons of each year over Hyderabad are shown in Figure 7. In the winter of each year, the CCM2 reasonably reproduces the observed variability of O_3 throughout the troposphere. During the premonsoon season of the years 2006 and 2007, the CCM2 simulations show good agreement with MOZAIC in the lower troposphere (below 5 km). In the middle and upper troposphere (5–11 km), the simulations underestimated the observations with biases of up to 20 ppbv during 2006 and 2007. On the other hand, during the premonsoon season of 2008, the simulations overestimated MOZAIC in the lower troposphere but showed a reasonably good match in the middle and upper troposphere. During the monsoon period of each year, the CCM2 consistently underestimated the observations with biases of up to 10–15 ppbv in the lower free troposphere. In this season, the agreement between model and observations in the upper troposphere is good except for 2008 when a sharp decline by about 10 ppbv at 9–11 km was not captured. In the postmonsoon season of 2006 and 2008, except for the tendency to overestimate O_3 in the lower and upper troposphere, the CCM2 simulations fairly reproduced the observations. However, the postmonsoon simulations for 2007 captured the features of O_3 variability in the lower and upper troposphere but failed to reproduce the layer of enhanced O_3 observed in the middle troposphere. Overall, the agreement between the observation and model varies from season to season and year to year.

The box-whisker plots of mixing ratio of O_3 observed in the different regions of the troposphere (0–2 km, 2–4 km, 4–6 km, 6–8 km, 8–10 km, and 10–12 km) are shown in Figure 8. The seasonal variation was strongest and more systematic in the lower troposphere but becomes weaker with increasing altitude. The year-to-year variations of O_3 were particularly significant in the lower and upper troposphere but were small in the middle troposphere. In the upper troposphere, the monthly mixing ratios of O_3 during the March–May period of 2006 were higher than the values in the same period of 2007 and 2008. In the entire troposphere, the monthly mean mixing ratio of O_3 showed a minimum in August of each year. However, the period of maxima in O_3 showed altitudinal dependency and varied from year to year. The monthly maxima were mostly observed during premonsoon season throughout the troposphere. During February–May, the mixing ratios of O_3 in the upper troposphere show enhancements of 60–80 ppbv in 2006 but low values of 30–50 ppbv were observed in 2007. On the other hand, between 10 and 12 km, the levels of O_3 (30–40 ppbv) during July–November of 2007 were lower by 10–15 ppbv compared to the same period in 2006 and 2008.

In Figure 8, the monthly mean CCM2 simulations of O_3 are also plotted for comparison. In a first approximation, the monthly simulations tend to capture the seasonality observed in the mixing ratio of O_3 in the different regions of the troposphere. In the lower troposphere, between 0 and 6 km, CCM2 agrees well with the observations. In the upper troposphere, CCM2 underestimates the observations during winter and premonsoon seasons. Overall, the simulated monthly mixing ratios of O_3 show smaller seasonal and year-to-year variations in the upper troposphere. The time series of $(O_3)_{CCM2}/(O_3)_{MOZAIC}$ ratios in the different regions of the troposphere during 2006–2008 are plotted in Figure 9. The monthly ratios of $(O_3)_{CCM2}/(O_3)_{MOZAIC}$ show large variability depending on the altitude. Typically, the agreement is good in the winter season every year. On the other hand, the model tends to underestimate and overestimate the observations in the premonsoon and monsoon seasons, respectively. The disagreement between observation and model could partly be attributed to the rather coarse resolution of CCM2. The other causes of disagreement could be the uncertainty in the parameterization of convection and quantification of NOx emissions in the tropical troposphere [*Folkins and Martin*, 2005; *Kunhikrishnan et al*., 2006]. Chemical transport model based studies have also reported a large range of biases in other urban regions of Europe and Asia mainly due to the coarse resolution [*Chen et al*., 2009; *Ordonez et al*., 2010; *Sahu et al*., 2013b]. The differences in the simulation of O_3 by different models can be attributed to the VOCs chemistry scheme and differences in emissions data sets.

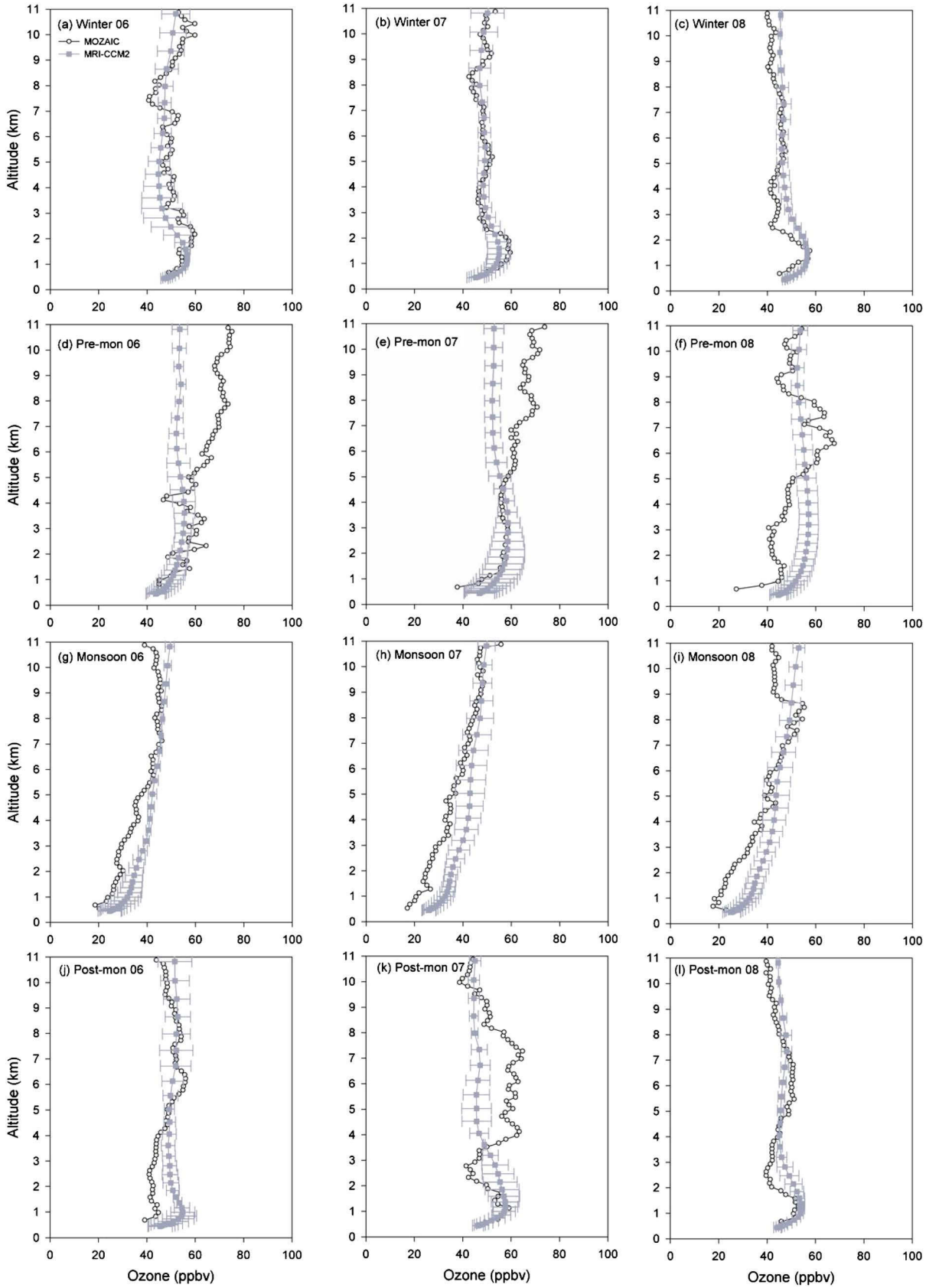

Figure 7. Comparison between the MOZAIC and MRI-CCM2 profiles of O_3 over Hyderabad during the different seasons of 2006–2008.

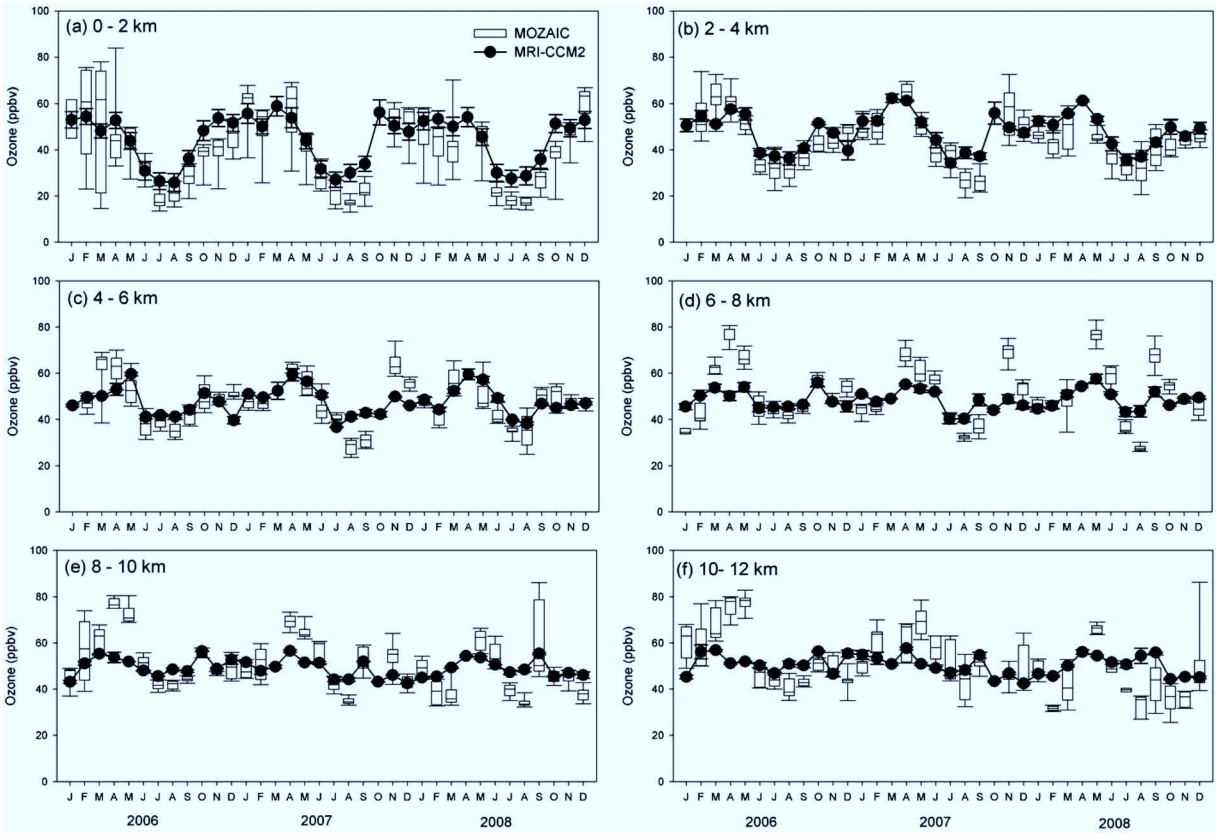

Figure 8. The monthly mixing ratios of O_3 using MOZAIC data in the different regions of the troposphere over Hyderabad during 2006–2008. The MRI-CCM2 simulations are also plotted for the comparison.

6. Discussion

6.1. Role of Biomass Burning and Long-Range Transport

The fire counts detected by the satellite-based Along Track Scanning Radiometer (ATSR) instruments have been used to investigate the spatiotemporal variation of biomass burning. The fire count map represents the location and time of the emitted radiances exceeding the criteria values in the middle infrared (MIR) band centered at 3.7 μm. The fire count algorithm based on the anomalous nighttime brightness temperature exceeding a threshold value of 308 K has been used in the present study. Further details of the ATSR

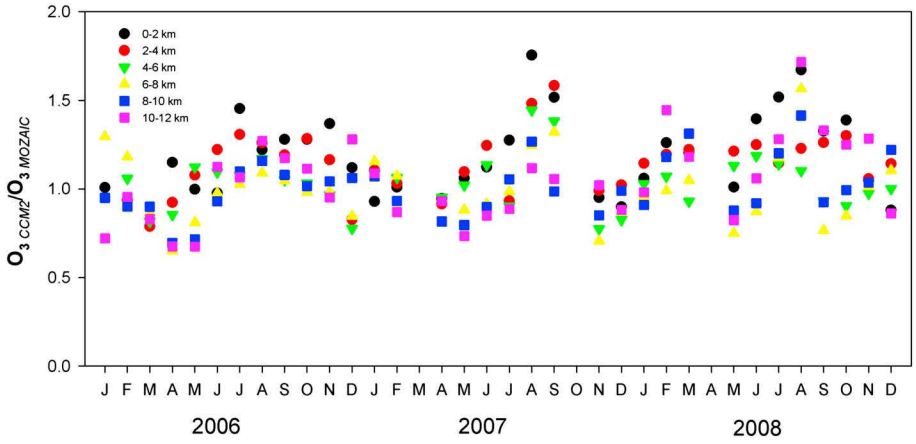

Figure 9. The monthly ratios of $(O_3)_{CCM2}/(O_3)_{MOZAIC}$ in the different regions of the troposphere over Hyderabad during 2006–2008.

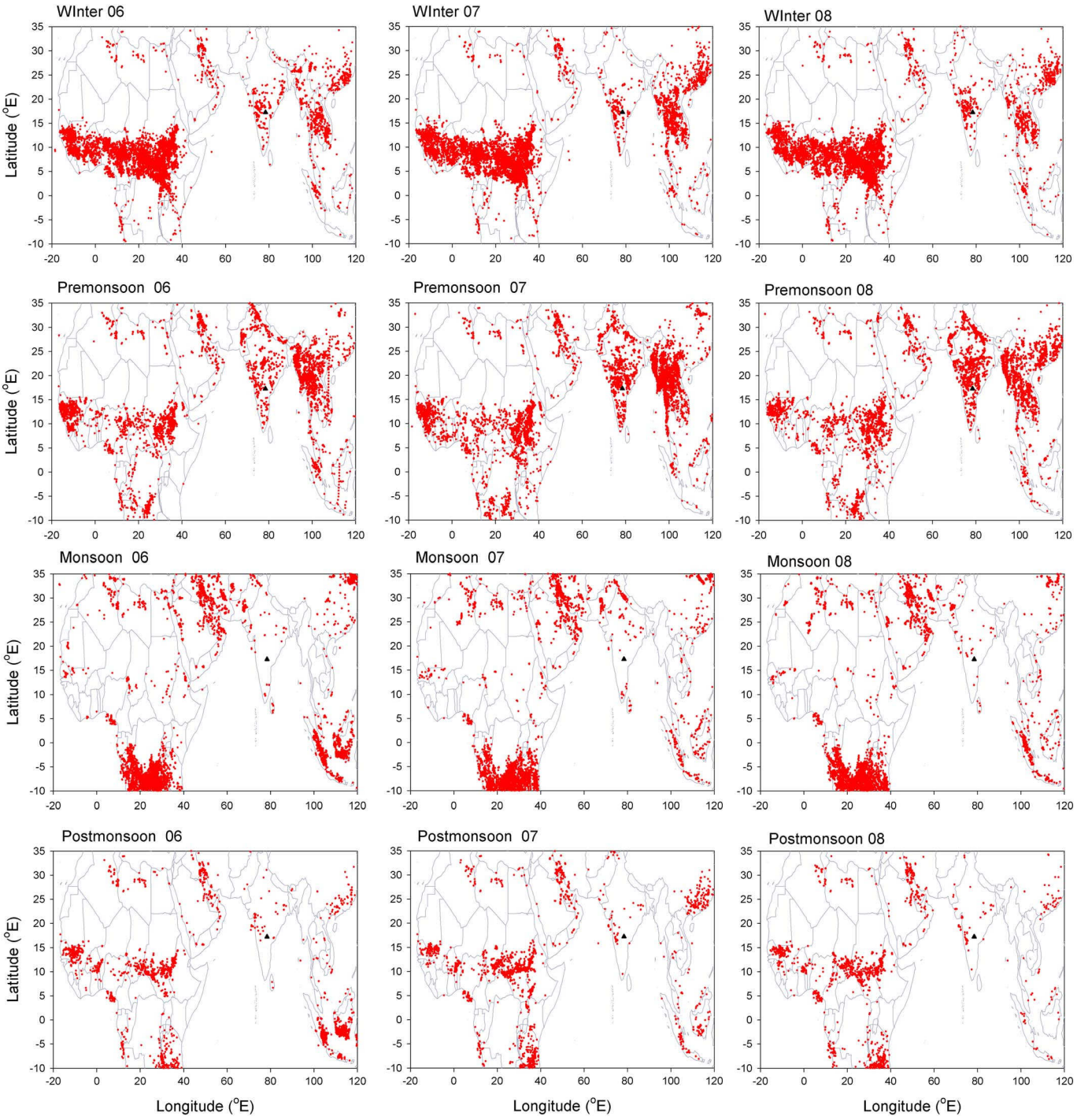

Figure 10. The ATSR fire count maps for India and surrounding continental regions during different seasons of 2006–2008.

detection and related methodologies can be found elsewhere [*Buongiorno et al.*, 1997; *Arino et al.*, 2001]. The seasonal fire count maps for India and surrounding continental regions are shown in Figure 10. The description of the season in the following discussion may not hold true for the other fire active regions but has been used as reference. In the winter season, the activities of biomass burning were most extensive in central Africa but were moderate in peninsular India and SE-Asia. In the premonsoon season, the major fire activities shifted to the Northern Hemisphere of S-SE Asia (e.g., India, Thailand, Burma, etc.). Typically, biomass burning during March–May accounted for more than 75% of total annual fire counts detected over India.

In the monsoon season, the activities of biomass burning were negligible over central Africa and northern hemispheric parts of S-SE Asia. In the monsoon and postmonsoon season, the fire counts detected over the southern hemispheric parts of S-SE Asia are mainly due to the forest and peat fires in Indonesia and Malaysia. The peat fires make the highest contribution among the other categories of biomass burning in Indonesia [*Langmann and Heil*, 2004]. The biomass burning activities detected over Indonesia and Malaysia during the monsoon and postmonsoon seasons in 2006 were much higher than the same period of 2007 and 2008. On the other hand, the fire counts detected over India during the premonsoon season in 2006 were much smaller than the same period of the years 2007 and 2008. The interannual differences in biomass burning were caused mainly by the transition from El Niño to La Niña conditions from 2006 to 2008 [*Sahu and Sheel*, 2013]. Though mainly detected over the Arabian Peninsula, the ATSR data also contains a number of events from nonbiomass burning like flares from oil-gas industrial sites and crude oil production throughout the year.

The monthly biomass burning emission estimates of CO, NOx, and ATSR fire count data over S-SE Asia during 2006–2008 are plotted in Figure 11. In this study, the emission data of CO and NOx were taken from the GFED3 inventory [*van der Werf et al*., 2006, 2010]. Typically, both emission and fire data show bimodal seasonality with the primary peak during February–May and secondary peak during July–September. The primary peak is mainly due to biomass burning in the northern hemispheric parts of S-SE Asia while the secondary peak is attributed to the southern hemispheric parts of S-SE Asia. However, exceptionally high and low emissions of trace gases during October–November of 2006 and 2008 were caused by the prevailing El Niño and La Niña conditions, respectively. In India, biomass burning occurs from February to May but the months of March and April experience the highest activity. Overall, the distribution of biomass burning emissions over S-SE Asia shows large regional, seasonal, and interannual variations. The variability in biomass burning emissions could also be an important factor to explain the higher O_3 variability during the premonsoon and postmonsoon seasons. However, the impact of nonlocal emissions in the vertical distribution of O_3 over Hyderabad depends on the pattern of long-range transport.

We have used the back trajectory model data to track the origin and long-range transport of air masses over Hyderabad. The isentropic back trajectories were calculated using the Japanese 25 year Reanalysis data (JRA-25, 6 h, $1.25^o \times 1.25^o$) [*Onogi et al*., 2007]. The Japan Meteorological Agency Climate Data Assimilation System (JCDAS) analysis data have been operational since 2005 and used in the present study. The JCDAS uses the common technique as JRA-25, but since it is operational day-by-day, only real-time observation data were assimilated. The advection algorithm used in the trajectory model is the same as reported in *Draxler and Hess* [1997]. For this study, back trajectories were calculated for a total run time of 7 days at 1 km, 5 km, and 10 km altitudes with a time step of 5 min. As shown in Figure 12, the origin and pathway of trajectories arriving over Hyderabad show very clear seasonal variation and also interannual to some extent.

Except for the monsoon season, the back trajectories arriving at 1 km show transport of continental flow mainly from the NE direction. The trajectories at 1 km were traced to have originated or passed through the polluted IGP during the winter, premonsoon, and postmonsoon seasons. In the monsoon season, the lower troposphere is influenced by the transport of cleaner air from the Arabian Sea and the Indian Ocean due to the prevailing winds from the SW direction. The flow of cleaner marine air is one of the major causes for the lower levels of O_3 over Hyderabad. The back trajectories at 5 km in the monsoon season show NW flow of air from Afghanistan and Pakistan. In other seasons, the back trajectories at this height originated over Africa and traveled through the Middle East and the Arabian Peninsula before arriving over Hyderabad. The back trajectories arriving at 10 km originated over the fire active region of central Africa and passed over the oceanic regions of the Arabian Sea and the Indian Ocean during winter and premonsoon seasons. Therefore, during these two seasons, the long-range transport of polluted air from fire active regions resulted in enhanced mixing ratios of O_3 in the upper troposphere over Hyderabad. In the postmonsoon season of 2006, the trajectories originating over central Africa seem to be predominant in the upper troposphere. On the other hand, the trajectories for the postmonsoon season of 2007 and 2008 indicate transport of mixed air from SE-Asia and the Arabian Sea. In the postmonsoon season of 2006, the combined analysis of both fire count and back trajectory data suggests transport of higher levels of O_3 precursors in the free troposphere from the fire active regions of Africa and Indonesia compared to other years. In summary, the year-to-year variation in the pattern of long-range transport was mostly noticed in the upper troposphere. In the tropical region, the interplay between convective and nonconvective processes can explain many aspects of seasonal

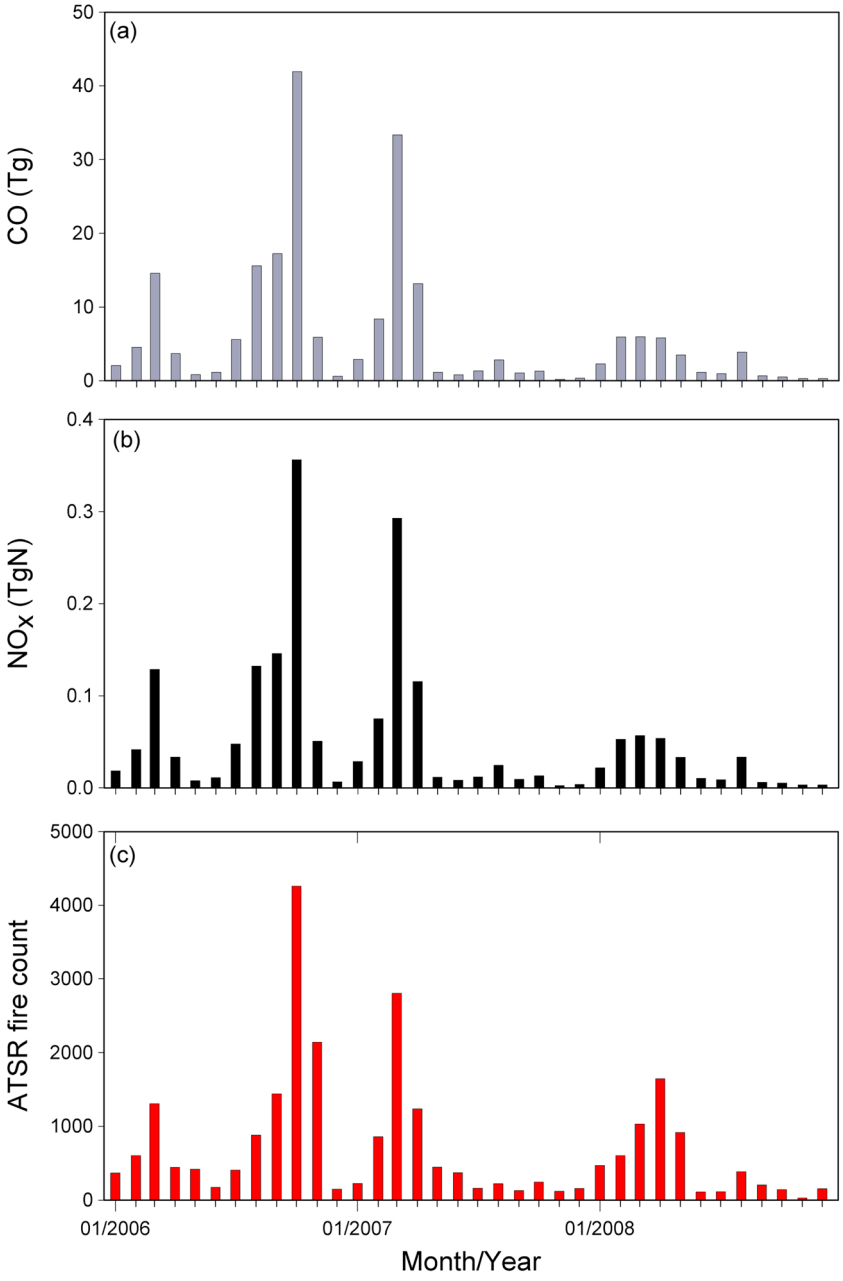

Figure 11. The monthly emissions of CO, NOx, and fire count data over S-SE Asia during 2006–2008.

and interannual distributions of trace species [*Hess*, 2005]. The role of convection in the distribution of O_3 has been investigated in the following subsection (section 6.2).

6.2. Role of Tropical Convection in O_3 Distribution

There are still major uncertainties regarding the roles of key atmospheric processes controlling the tropospheric O_3 budget [*Lawrence et al.*, 2003]. The major atmospheric processes are advection, convection, and chemical production and loss of O_3. Field observations have shown efficient redistribution of tropospheric O_3 by tropical convection [*Choi et al.*, 2005; *Sahu and Lal*, 2006]. According to the estimates, there can be about 30% increase in the tropospheric column O_3 (TCO) due to convective transport of precursors in the upper troposphere [*Pickering et al.*, 1992]. On the other hand, the downdrafts of O_3-rich air from the free troposphere to the boundary layer can result in a net decrease of TCO [*Sahu and Lal*, 2006]. The standard meteorological parameters like temperature, pressure, and RH are not conserved during the

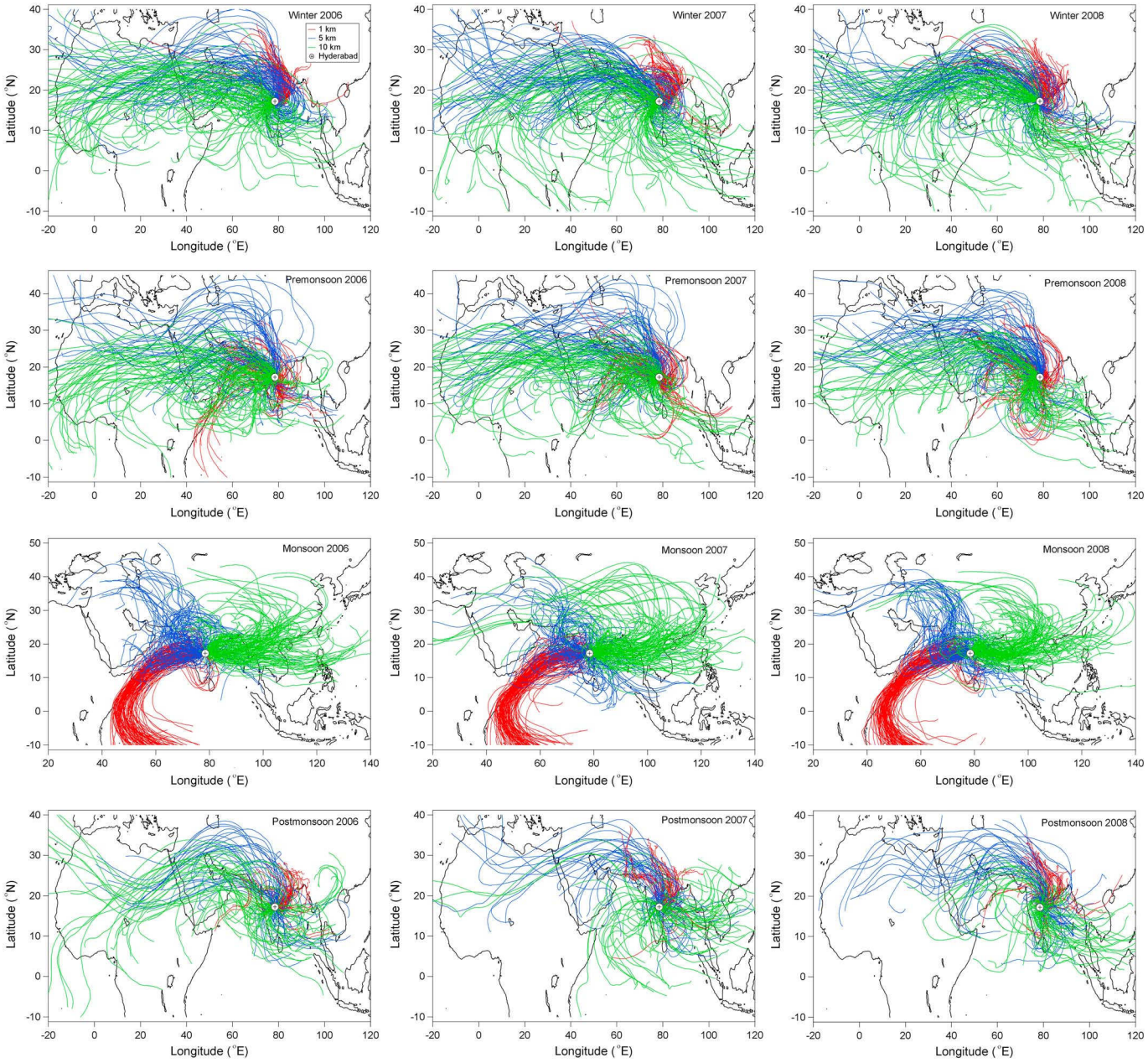

Figure 12. The 7 day back trajectory plots at 1 km, 5 km, and 10 km of altitudes over Hyderabad (encircled symbol) during the different seasons of 2006–2008.

convective transport. However, θ_e remains conserved during both dry and moist adiabatic processes [*Betts et al.*, 1992; *Sahu et al.*, 2013b]. Climatologically, the tropical lower troposphere is characterized by a decrease in θ_e and an increase in O_3 with altitude [*Folkins et al.*, 1999; *Betts et al.*, 2002]. The vertical profile of lapse rate (LR) has been used to investigate the local stability of air masses as θ_e does not always reflect the local stability conditions. Nonetheless, we have calculated the profiles of both θ_e and LR over Hyderabad using MOZAIC data from the following equations.

$$\mathrm{EPT}(\theta_e) = \left(T + \frac{q \times L}{C_p}\right) \times \left(\frac{p_0}{p}\right)^{\frac{R}{C_p}} \quad (1)$$

$$\text{Lapse Rate (LR)} = \left(\frac{dT}{dz}\right) \quad (2)$$

Where parameters are; T = temperature, q = specific humidity, p_0 = pressure at surface, p = pressure at altitude (z), L = latent heat (2.54×10^6 J Kg^{-1}), R = universal gas constant (287 J K^{-1}), and C_p = specific heat capacity (1004 J K^{-1}). As given below, the value of θ_e increases and decreases with height in convectively stable and unstable atmospheric systems, respectively.

$$\frac{\partial \theta_e}{\partial z} > 0 \Rightarrow \text{covectively stable}$$
$$\frac{\partial \theta_e}{\partial z} = 0 \Rightarrow \text{covectively neutral}$$
$$\frac{\partial \theta_e}{\partial z} < 0 \Rightarrow \text{convectively unstable}$$

The measured profiles of LR can be useful to study the low-level circulations in convectively active regions [*Folkins et al.*, 2008]. The static stability is closely related to LR in the lower troposphere. The minimum of θ_e is marked as the melting level which denotes a transition from a conditionally unstable to stable atmosphere [*Folkins and Martin*, 2005]. Typically, downdrafts detrain the air into the background atmosphere above the melting level, while entrainment occurs below the melting level [*Folkins*, 2006].

The average vertical profiles of θ_e, LR, and O_3 over Hyderabad for the all the seasons are shown in Figure 13. The potential stability conditions derived using θ_e in the different regions of the troposphere over Hyderabad are given in Table 2. Overall, the lower troposphere is potentially unstable due to the source of H_2O and strong solar heating. The melting level heights were at about 3.5 km, 5.5 km, 4.5 km, and 2.5 km during the winter, premonsoon, monsoon, and postmonsoon seasons, respectively. The melting level is associated with a local maximum in stability coinciding with the minimum in LR during all seasons over Hyderabad. The mixing ratio of O_3 and LR show anticorrelated vertical variation in the troposphere. The presence of O_3-poor stable layers are marked by the lower environmental LR than the moist (~6.5 K km^{-1}) and dry (~9.8 K km^{-1}) LR values. A layer of local maximum in LR just below the melting level is defined as the Melting Level Stability Anomaly (MLSA). The upward displacement and vertical depth of the MLSA vary with the season in response to the change in surface temperature. For example, a narrow layer (at ~1.5 km of altitude) and a broad layer (at ~2.5 km of altitude) of MLSA during winter and premonsoon seasons were due to the lower and higher surface temperatures, respectively. The mixing ratios of O_3 tend to increase slightly with increasing altitude in the MLSA layer. On the other hand, the mixing ratios of O_3 tend to decrease with altitude in the layer of static stability near the melting level. These features were less prominent during the monsoon seasons due to weaker static stability and MLSA. The layers of H_2O-rich and O_3-poor air suggest enhanced detrainment just above the PBL height due to cumulus congestus. On the other hand, the enhanced mixing ratios of O_3 above the melting level (4–8 km of altitudes) could be due to the entrainment of long-range transported O_3-rich air over Hyderabad.

The average θ_e values of 345–350 K at 9–11 km correspond to the convective outflow of surface air during the premonsoon and monsoon seasons [*Folkins et al.*, 1999]. In the upper troposphere, the environmental LR values of ~7.5–9.0 K km^{-1} are close to the dry adiabatic LR confirming the impact of convective outflow of PBL air mass during all the seasons. However, the mixing ratios of O_3 in the upper troposphere are significantly higher than the surface values, which indicate additional contributions from sources other than the direct transport of surface air. One of these sources could be the net photochemical production of O_3 due to the efficient transport of precursor gases from the PBL to the upper troposphere [*Pickering et al.*, 1992; *Kita et al.*, 2002]. In case of deep convection, depending on several meteorological conditions, vertical transport can redistribute the tropical troposphere in less than 1 h. The convective outflow of precursors from local sources, mainly from biomass burning in the premonsoon season, can enhance the photochemical formation of O_3 in the upper troposphere. This explanation agrees with the fact that the levels of O_3 in the upper troposphere were highest during the premonsoon season. The CCM2 simulations do not tend to capture the detailed features of tropospheric O_3 caused by convective motions over Hyderabad. The present results over Hyderabad agree with the climatological seasonal variations of the stable and unstable layers in the tropics [*Nodzu et al.*, 2006].

6.3. Impact of Local Meteorology on O_3

The local meteorology plays a large role in determining the dispersion, accumulation, and photochemistry of atmospheric O_3. Several meteorological parameters viz., temperature, RH, solar radiation, wind speed, and wind direction can influence the distribution of O_3 in the PBL region. Variations in the meteorological

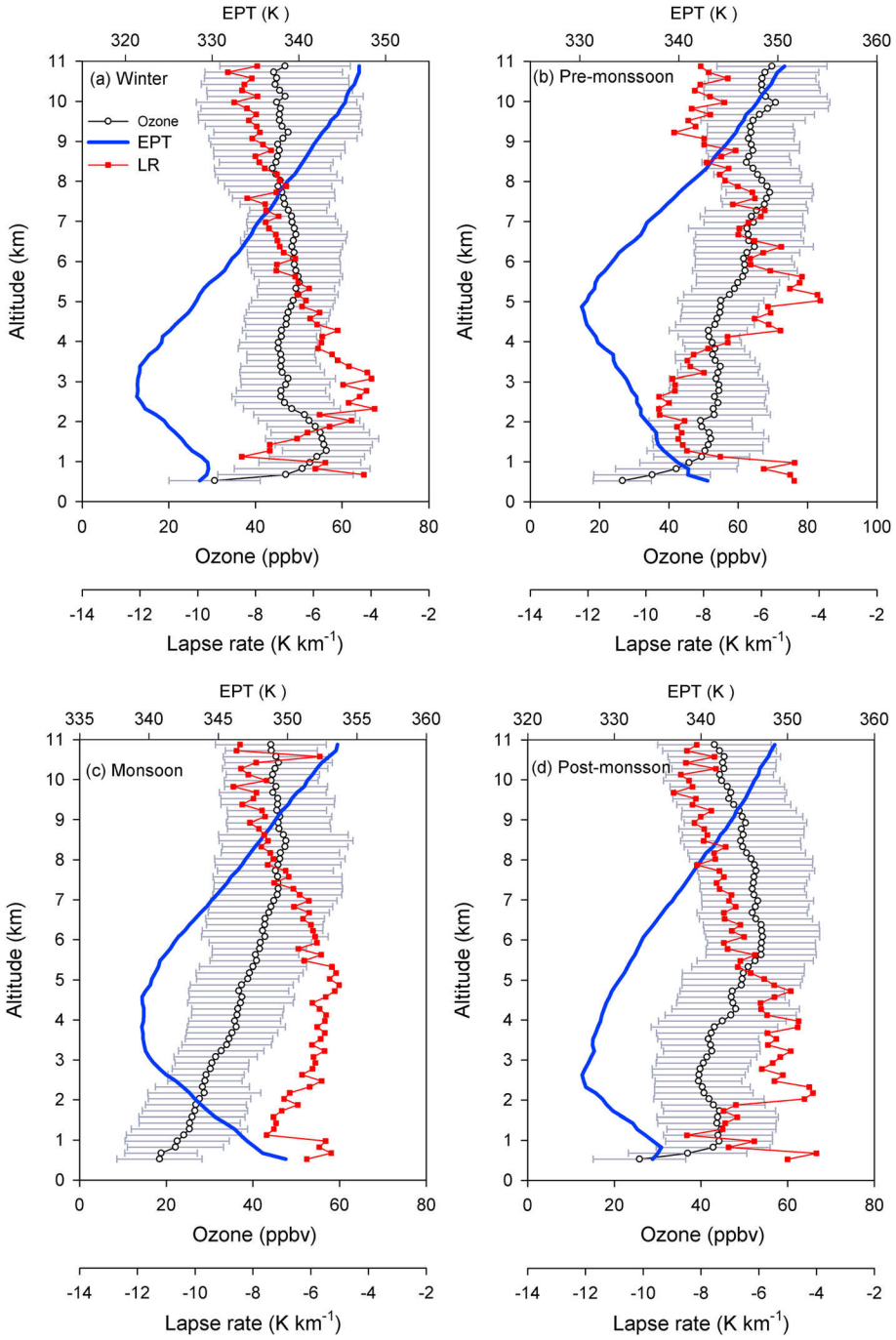

Figure 13. Seasonal mean vertical profiles of O_3, equivalent potential temperature (EPT, θ_e), and lapse rate (LR) using MOZAIC data over Hyderabad during 2006–2008.

parameters have been observed to play an important role in the seasonal distributions of various secondary pollutants in urban areas of India [*Swamy et al.*, 2012]. In a previous study, we have reported that the levels of O_3, CO, black carbon, and organic carbon show strong dependencies with the wind speed in Bangkok city [*Sahu et al.*, 2011, 2013a, 2013b]. Studies have reported on the role of local meteorology on the distribution of O_3 in other urban areas of the world [e.g., *Husar and Renard*, 1997; *Dueñas et al.*, 2002]. However, the quantitative estimate of contributions of different meteorological regimes requires detailed studies using regional scale models [*Verma et al.*, 2010].

Table 2. The Potential Stability Conditions Derived Using the Equivalent Potential Temperatures in the Different Regions of the Troposphere Over Hyderabad

	Layers (km) in the Troposphere			
Stability Condition	Winter	Premonsoon	Monsoon	Postmonsoon
$(\partial\theta_e/\partial z) < 0$	0–2.5	0–4.0	0–3.2	0–2.2
$(\partial\theta_e/\partial z) \approx 0$	2.5–3.5	4.0–5.5	3.2–5.0	2.2–4.2
$(\partial\theta_e/\partial z) > 0$	3.5–11	5.5–11	5.0–11	4.2–11

In this study, we have investigated the dependence of O_3 on wind parameters and RH in the lower troposphere (< 2 km). The wind polar diagrams, color coded with the mixing ratio of O_3, for the four different seasons are shown in Figure 14. In the winter season, the elevated mixing ratios of O_3 (> 50 ppbv) were mostly due to the prevailing winds from the NE regardless of the wind speed (Figure 14a). The NE and NW winds bring O_3-rich air from the polluted areas of Hyderabad city. However, occasionally in this season, the lower levels of O_3 were observed during the flow from the SE-SW sector. In the premonsoon and postmonsoon seasons, the calm wind seems to favor the local production of O_3 while the impact of dispersion could be noticed under the stronger wind flow. The higher surface temperature and accumulation of precursor gases emitted from local sources result in an increased rate of photochemical production of O_3 in the premonsoon season. The episodes of high O_3 under calm winds in the premonsoon season were more frequent compared to the other seasons due to widespread biomass burning in the surrounding areas of Hyderabad. In the monsoon

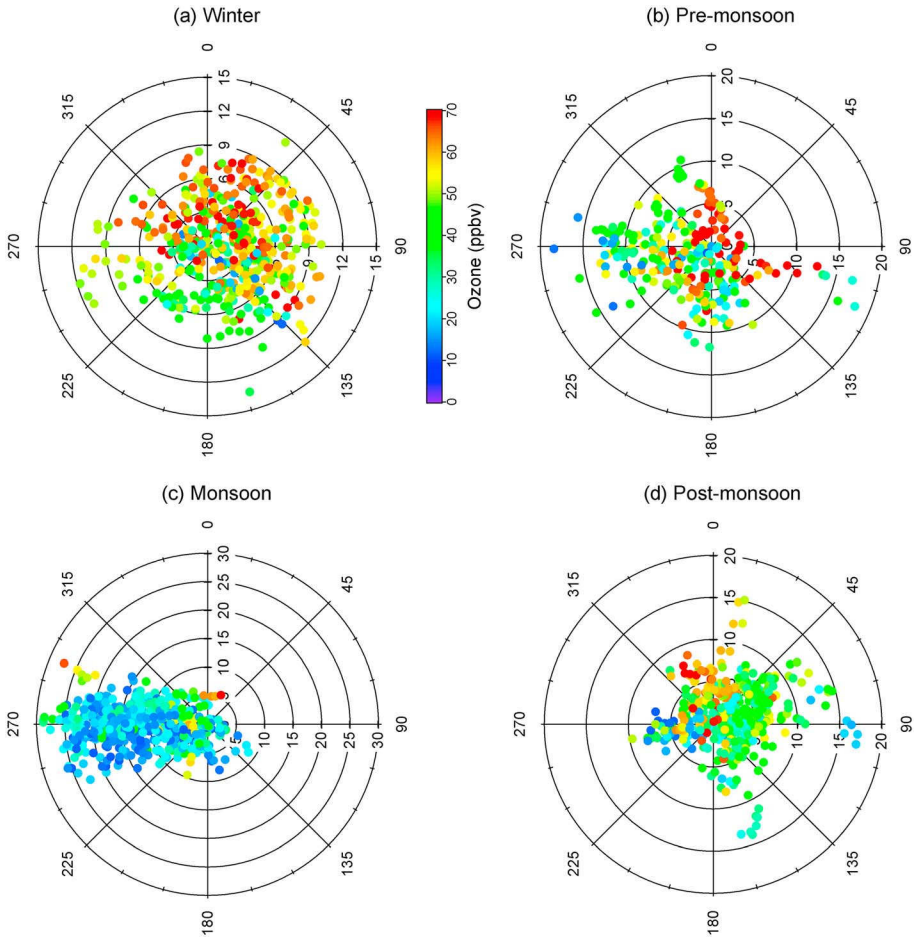

Figure 14. The polar plots using wind speed (wind speed, m s^{-1}) and wind direction (degree) data, coded with the mixing ratio of O_3, in the lower troposphere (< 2 km of altitudes) over Hyderabad during the different seasons of 2006–2008.

Table 3. The Average Mixing Ratios of Ozone in the Lower Troposphere (0–2 km) Over Hyderabad During the Different Seasons of the Years 2006–2008

	Average ± SD (ppbv)			
Wind Sector	Winter	Premonsoon	Monsoon	Postmonsoon
N-NE	57 ± 13	61 ± 16	47 ± 23	47 ± 12
E-NE	54 ± 11	62 ± 12	18 ± 7	42 ± 10
E-SE	52 ± 15	54 ± 21	25 ± 9	38 ± 12
S-SE	43 ± 14	40 ± 15	20 ± 9	36 ± 10
S-SW	42 ± 12	47 ± 17	30 ± 14	37 ± 19
W-SW	49 ± 11	42 ± 16	21 ± 11	34 ± 16
W-NW	53 ± 15	44 ± 13	26 ± 12	34 ± 19
N-NW	57 ± 12	55 ± 14	34 ± 13	53 ± 13

season, the mixing ratios of O_3 were mostly in the range of 10–35 ppbv without significant dependence on the wind speed. However, episodes of higher levels of O_3 were observed under calm wind conditions. In this season, the stronger winds (up to 30 m s^{-1}) consistently from the west suggest substantial impacts of dilution due to flow of marine air from the Arabian Sea. The statistics of O_3 for the different wind sectors in the lower troposphere over Hyderabad are presented in Table 3. During each season, the highest mixing ratios of O_3 were observed for winds from the northern sector (N-NW to N-NE) while values were lower for the winds from the southern sector (S-SW to S-SE).

Scatter plots of the mixing ratios of O_3 and wind speed for the four different wind sectors are plotted in Figure 15. The mixing ratio of O_3 tends to increase slightly with the increasing wind speed for flow from the eastern sector (NE and SE). For flow from the western sector (NW and SW), the mixing ratio of O_3 tends to increase with increasing wind speed in the lower wind flow regime (< 5 m s^{-1}). Under calm wind conditions, average mixing ratios of 37–41 ppbv observed during southerly flow were significantly lower than the values of 45–53 ppbv observed under northerly flow. The higher and lower background levels of O_3 are mainly due to prevailing northerly winter (continental air) and southerly summer (oceanic air) circulations, respectively. While O_3 decreased rapidly with increased wind speed under the strong wind regime (> 5 m s^{-1}) from the

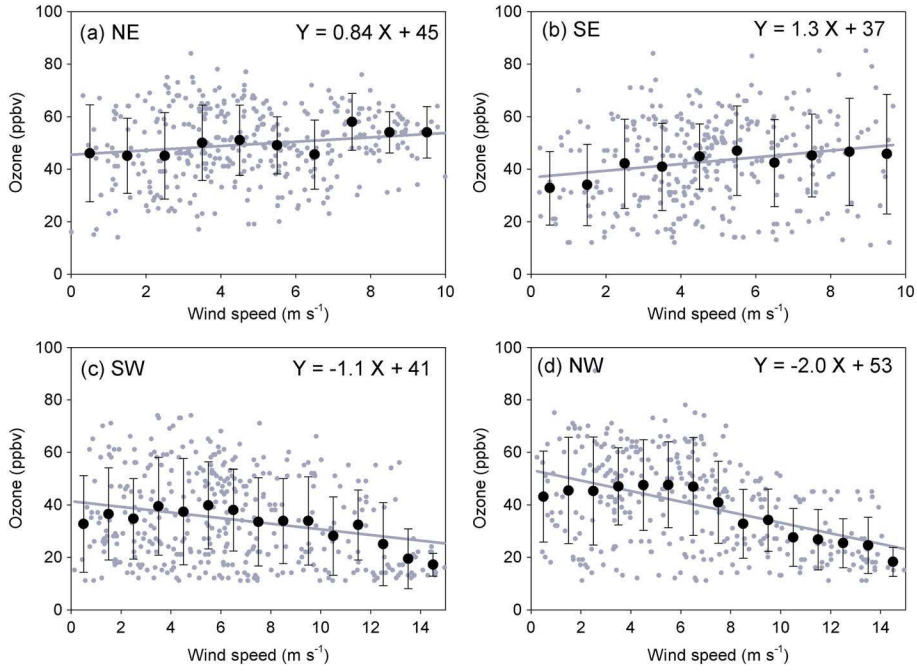

Figure 15. The scatter plots showing the dependencies of the mixing ratio of O_3 on wind speed in the lower troposphere (< 2 km of altitudes) over Hyderabad in the four different wind sector regimes.

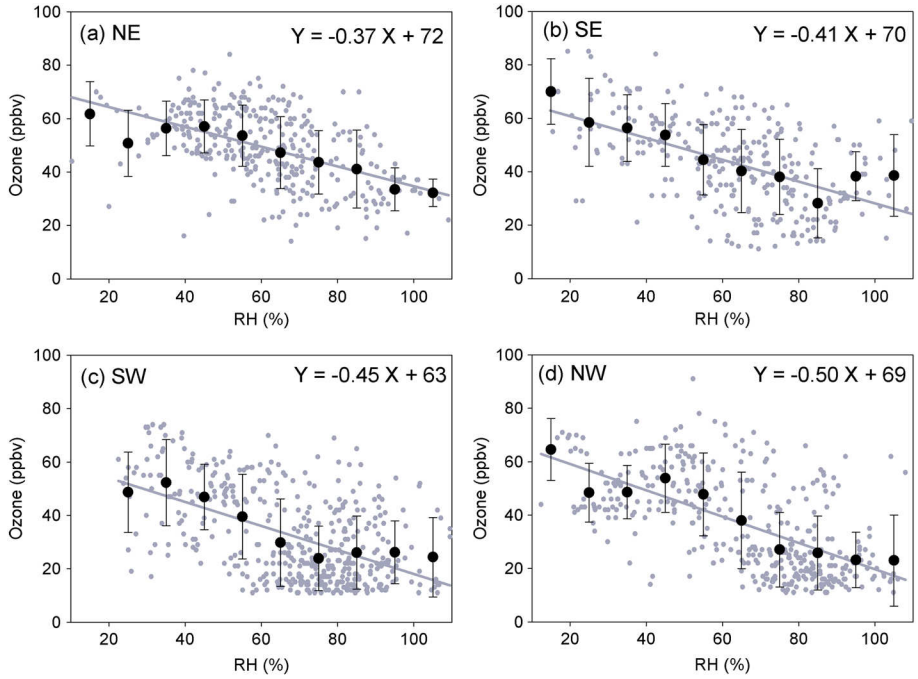

Figure 16. The scatter plots showing the dependencies of the mixing ratio of O_3 on relative humidity (RH) in the lower troposphere (< 2 km of altitudes) over Hyderabad in the four different wind sector regimes.

NW and SW directions, the regression analysis of O_3 versus wind speed (averaged for a bin of 1.0 m s^{-1}) shows good linear relation in the air masses from all wind sectors in the PBL region. The slopes of $\Delta O_3/\Delta$(wind speed) were 0.84 ppbv/m s^{-1} and 1.3 ppbv/m s^{-1} under flow from NE and SE sectors, respectively. On the other hand, values of $\Delta O_3/\Delta$(wind speed) were −1.1 ppbv/m s^{-1} and −2.0 ppbv/m s^{-1} under the SW and NW sectors, respectively.

We have also investigated the dependence of O_3 on RH in the PBL region. The regression fit of O_3 versus RH (averaged for a bin of 10%) shows good linear relation for all wind sectors (Figure 16). As evident from the intercept of linear regression fit in each sector, the mixing ratios of O_3 were highest in low RH regime over Hyderabad. The mixing ratio of O_3 declines rapidly with increasing RH regardless of the wind direction. The slopes of $\Delta O_3/\Delta$(RH) were 0.37, −0.41 −0.45, and −0.50 ppbv/RH (%) in the NE, SE, SW, and NW sectors, respectively. The decline of O_3 with both wind speed and RH were particularly significant during the wind flow from SW and NW directions. This can be interpreted as evidence of local source contributions, since higher levels of wind speed and RH cause increasing dilution/loss of local production of O_3. On the other hand, the increasing trend of O_3 with the wind speed during NE and SE flow could be due to the higher background levels of O_3 in the upwind region. In summary, the relation between O_3 and meteorological parameters varies from season to season over Hyderabad. Nonetheless, the actual origin of the regional O_3 is identified only vaguely through the statistical analysis of meteorological parameters.

7. Summary and Conclusions

Characteristics of tropospheric O_3 variability over Hyderabad city in India have been studied based on the MOZAIC measurements, back trajectories, fire counts, and meteorological data. In the PBL region, the mixing ratio of O_3 shows strong seasonal variation with highest and lowest values during the winter and monsoon seasons, respectively. In the free troposphere, the distribution of O_3 shows a slight shift in the seasonal pattern as the highest and lowest values were observed in the premonsoon and monsoon seasons, respectively. The seasonal variation of H_2O concentration appears to be opposite in phase to that of O_3 over Hyderabad. In the free troposphere, the seasonality of wind speed is similar to that of O_3 but opposite to that of H_2O. Layers of enhanced O_3 were associated with lower values of both wind speed and RH in the middle

troposphere. The study region is influenced by the flow of cleaner marine air from the SW in the monsoon season while the winds from NE and NW transport the continental pollutants during the other seasons. Moreover, the activities of biomass burning were negligible over the northern hemispheric parts of S-SE Asia in the monsoon season. During the winter season, the activities of biomass burning were extensive in Africa but moderate in peninsular India. In the premonsoon season, the major biomass burning activities were detected over India, Thailand, and Burma. In the monsoon and postmonsoon season, significant activities of biomass burning were detected over the island of Indonesia and Malaysia.

The mixing ratios of O_3 were highest and lowest during 2006 and 2008, respectively. In the upper troposphere, the year-to-year variation of O_3 was positively correlated with wind speed but showed negative correlation with RH. In 2006, enhanced levels of O_3 in the upper troposphere were associated with strong wind shears and hence inhibited deep convection over Hyderabad. On the other hand, lower values of O_3 in 2008 were associated with the weaker wind shear and hence strong deep convection. In addition, the impact of year-to-year differences in biomass burning caused by the transition from the El Niño to La Niña conditions was also observed.

The CCM2 simulations of O_3 reasonably reproduced the observed variability in the troposphere over Hyderabad. The agreement between CCM2 and MOZAIC was good in the winter season during all the years. However, the model tends to underestimate and overestimate the observations in the premonsoon and monsoon seasons, respectively. The monthly ratios of $(O_3)_{CCM2}/(O_3)_{MOZAIC}$ varied in the range of 0.7–1.8 in the different regions of troposphere. Overall, the agreement between the MOZAIC observation and CCM2 simulation varied from season to season and year to year. The MOZAIC data are useful to reduce uncertainty in the vertical convective mixing and net chemical production and loss of O_3 simulated by models.

We have investigated the roles of convective transport and local stability in the vertical variation of O_3 using the MOZAIC profiles of equivalent potential temperature and lapse rate over Hyderabad. The mixing ratio of O_3 and lapse rate show anticorrelated variation in the troposphere. The lower levels of O_3 were observed in the stable layers marked by lower environmental lapse rates. The layers of O_3-poor air were due to the enhanced detrainment in the lower troposphere associated with cumulus congestus. In the middle troposphere, the layers of enhanced mixing ratios of O_3 could be due to the entrainment of long-range transport mainly from fire active regions of Africa.

The mixing ratio of O_3 depends on local meteorology in the PBL region, but no clear dependencies were observed in the free troposphere. Typically, the higher mixing ratios of O_3 were observed under the wind flow from the northern sector and lower values during southerly winds. The positive slope $\Delta O_3/\Delta$(wind speed) values of 0.84–1.3 ppbv m s^{-1} under easterly flow indicate increasing levels of O_3 with the increasing wind speed. On the other hand, the negative slope $\Delta O_3/\Delta$(wind speed) values under westerly wind flow indicate decreasing levels of O_3 with the increasing wind speed over Hyderabad. In the PBL region, the increase and decrease in the mixing ratios of O_3 with increasing wind speed were associated with the transport from polluted and cleaner regions, respectively. The mixing ratio of O_3 declined rapidly with the increasing level of RH. The decline of O_3 with both wind speed and RH were particularly significant during the westerly wind flow over Hyderabad. Overall, the profiles of O_3 show large variability on different time scales over the continental tropical region and both atmospheric dynamic and biomass burning emissions play major roles in the distribution.

Acknowledgments

The authors acknowledge for their strong support the European Commission, Airbus, CNRS-France, FZJ-Germany, and the airlines (Lufthansa, Air France, Austrian, and former Sabena who carry free of charge the MOZAIC instrumentation since 1994). The ATSR World Fire Atlas data have been taken from Ionia products of European Space Agency. The MACCity and GFED3 data sets were downloaded from the Ether/ECCAD database. This work was partly supported by JSPS KAKENHI grant 24740325.

References

Akimoto, H. (2003), Global air quality and pollution, *Science*, *302*, 1716–1719, doi:10.1126/science.1092666.

Allan, R., J. Lindesay, and D. E. Parker (1996), *El Niño Southern Oscillation and Climatic Variability*, 416 pp., CSIRO, Collingwood, Victoria, Australia.

Arino, O., M. Simon, I. Piccolini, and J. M. Rosaz (2001), The ERS-2 ATSR-2 World Fire Atlas and the ERS-2 ATSR-2 World Burnt Surface Atlas projects, paper presented at 8th ISPRS conference on Physical Measurement and Signatures in Remote Sensing, European Space Agency, Aussois, France.

Asnani, G. C. (2005), Climatology of the tropics, in *Tropical Meteorology*, vol. 1, pp. 100–204, G. C. Asnani, Pune, India.

Bansod, S. D. (2011), Interannual variability of convective activity over the tropical Indian Ocean during the El Niño/La Niña events, *Int. J. Remote Sens.*, *32*(19), 5565–5582.

Barret, B., E. Le Flochmoen, B. Sauvage, E. Pavelin, M. Matricardi, and J. P. Cammas (2011), The detection of post-monsoon tropospheric ozone variability over south Asia using IASI data, *Atmos. Chem. Phys.*, *11*, 9533–9548.

Betts, A. K., R. L. Desjardins, and J. I. MacPherson (1992), Budget analysis of the boundary layer grid flights during FIFE 1987, *J. Geophys. Res.*, *97*, 18,533–18,546.

Betts, A. K., L. V. Gatti, A. M. Cordova, M. A. F. Silva Dias, and J. Fuentes (2002), Transport of ozone to the surface by convective downdrafts at night, *J. Geophys. Res.*, *107*(1), 8046, doi:10.1029/2000JD000158.

Buongiorno, A., O. Arino, C. Zehner, P. Colagrande, and P. Goryl (1997), ERS-2 monitors exceptional fire event, *Earth Obs. Q.*, *56*, 1–6.

Burrows, J. P., et al. (1999), The Global Ozone Monitoring Experiment (GOME): Mission concept and first scientific results, *J. Atmos. Sci.*, *56*, 151–175.

Chan, C. Y., L. Y. Chan, W. L. Chang, Y. G. Zheng, H. Cui, X. D. Zheng, Y. Qin, and Y. S. Li (2003), Characteristics of a tropospheric ozone profile and implications for the origin of ozone over subtropical China in the spring of 2001, *J. Geophys. Res.*, *108*(D20), 8800, doi:10.1029/2003JD003427.

Chen, D., Y. Wang, M. B. McElroy, K. He, R. M. Yantosca, and P. Le Sager (2009), Regional CO pollution and export in China simulated by the high-resolution nested-grid GEOS-Chem model, *Atmos. Chem. Phys.*, *9*, 3825–3839.

Choi, Y., Y. Wang, T. Zeng, R. V. Martin, T. P. Kurosu, and K. Chance (2005), Evidence of lightning NOx and convective transport of pollutants in satellite observations over North America, *Geophys. Res. Lett.*, *32*, L02805, doi:10.1029/2004GL021436.

Cooper, M. J., R. V. Martin, N. J. Livesey, D. A. Degenstein, and K. A. Walker (2013), Analysis of satellite remote sensing observations of low ozone events in the tropical upper troposphere and links with convection, *Geophys. Res. Lett.*, *40*, 3761–3765, doi:10.1002/grl.50717.

Cooper, O. R., et al. (2006), Large upper tropospheric ozone enhancements above midlatitude North America during summer: In situ evidence from the IONS and MOZAIC ozone measurement network, *J. Geophys. Res.*, *111*, D24S05, doi:10.1029/2006JD007306.

Cooper, O. R., et al. (2010), Increasing springtime ozone mixing ratios in the free troposphere over western North America, *Nature*, *463*, 344–348, doi:10.1038/nature08708.

Deushi, M., and K. Shibata (2011), Development of a Meteorological Research Institute Chemistry Climate Model version 2 for the study of tropospheric and stratospheric chemistry, *Pap. Meteorol. Geophys.*, *62*, 1–46, doi:10.2467/mripapers.62.1.

Draxler, R. R., and G. D. Hess (1997), Description of the HYSPLIT_4 modeling system, *NOAA Tech. Memo. ERL ARL-224*, 24 pp.

Dueñas, C., M. C. Fernández, S. Cañete, J. Carretero, and E. Liger (2002), Assessment of ozone variations and meteorological effects in an urban area in the Mediterranean coast, *Sci. Total Environ.*, *299*, 97–113, doi:10.1016/S0048-9697(02)00251-6.

Emberson, L. D., M. Ashmore, and F. Murray (2003), *Air Pollution Impacts on Crops and Forests: A Global Assessment*, Air Pollut. Rev., vol. 4, 372 pp., Imperial Coll. Press, London.

Fishman, J., K. Fakhruzzaman, B. Cros, and D. Nganga (1991), Identification of widespread pollution in the Southern Hemisphere deduced from satellite analyses, *Science*, *252*, 1693–1696.

Folkins, I. (2006), Convective damping of buoyancy anomalies and its effect on lapse rates in the tropical lower troposphere, *Atmos. Chem. Phys.*, *6*, 1–12, doi:10.5194/acp-6-1-2006.

Folkins, I., and R. V. Martin (2005), The vertical structure of tropical convection and its impact on the budgets of water vapor and ozone, *J. Atmos. Sci.*, *62*, 1560–1573.

Folkins, I., et al. (1999), A barrier to vertical mixing at 14 km in the tropics: Evidence from ozonesondes and aircraft measurements, *J. Geophys. Res.*, *104*, 22,095–22,102.

Folkins, I., C. Braun, A. M. Thompson, and J. C. Witte (2002), Tropical ozone as in indicator of deep convective outflow, *J. Geophys. Res.*, *107*(D13), 4184, doi:10.1029/2001JD001178.

Folkins, I., S. Fueglistaler, G. Lesins, and T. Mitovski (2008), A low-level circulation in the tropics, *J. Atmos. Sci.*, *65*, 1019–1034, doi:10.1175/2007JAS2463.1.

Forster, P. M., and K. P. Shine (1997), Radiative forcing and temperature trends from stratospheric ozone changes, *J. Geophys. Res.*, *102*, 10,841–10,856.

Gauss, M., et al. (2003), Radiative forcing in the 21st century due to ozone changes in the troposphere and the lower stratosphere, *J. Geophys. Res.*, *108*(D9), 4292, doi:10.1029/2002JD002624.

Ghude, S. D., G. G. Pfister, C. Jena, R. J. van der A, L. K. Emmons, and R. Kumar (2013), Satellite constraints of nitrogen oxide (NOx) emissions from India based on OMI observations and WRF-Chem simulations, *Geophys. Res. Lett.*, *40*, 1–6, doi:10.1029/2012GL053926.

Girishkumar, M. S., and M. Ravichandran (2012), The influences of ENSO on tropical cyclone activity in the Bay of Bengal during October–December, *J. Geophys. Res.*, *117*, C02033, doi:10.1029/2011JC007417.

Granier, C., et al. (2011), Evolution of anthropogenic and biomass burning emissions of air pollutants at global and regional scales during the 1980–2010 period, *J. Clim.*, *109*, 163–190, doi:10.1007/s10584-011-0154-1.

Heald, C. L., D. J. Jacob, P. I. Palmer, M. J. Evans, G. W. Sachse, H. B. Singh, and D. R. Blake (2003), Biomass burning emission inventory with daily resolution: Application to aircraft observations of Asian outflow, *J. Geophys. Res.*, *108*(D21), 8811, doi:10.1029/2002JD003082.

Helten, M., H. G. J. Smit, D. Kley, J. Ovarlez, H. Schlager, R. Baumann, U. Schumann, P. Nedelec, and A. Marenco (1999), In-flight intercomparison of MOZAIC and POLINAT water vapor measurements, *J. Geophys. Res.*, *104*, 26,087–26,096.

Hess, P. G. (2005), A comparison of two paradigms: The relative global roles of moist convective versus nonconvective transport, *J. Geophys. Res.*, *110*, D20302, doi:10.1029/2004JD005456.

Horowitz, L. W., et al. (2003), A global simulation of tropospheric ozone and related tracers: Description and evaluation of MOZART, version 2, *J. Geophys. Res.*, *108*(D24), 4784, doi:10.1029/2002JD002853.

Husar, R. B., and W. P. Renard (1997), Ozone as a function of local wind speed and direction: Evidence of local and regional transport, paper presented at the Air and Waste Management Association's 90th Annual Meeting and Exhibition, Toronto, Ontario, 8–13 June 1997.

Intergovernmental Panel on Climate Change (IPCC) (2013), *Climate Change 2013: The Physical Science Basis*, Contribution of Working Group I to the Fifth Assessment Report of the Intergovernmental Panel on Climate Change, Cambridge Univ. Press, New York.

Kajino, M., M. Deushi, T. Maki, N. Oshima, Y. Inomata, K. Sato, T. Ohizumi, and H. Ueda (2012), Modeling wet deposition and concentration of inorganics over Northeast Asia with MRI-PM/c, *Geosci. Model Dev.*, *5*, 1363–1375, doi:10.5194/gmd-5-1363-2012.

Kita, K., et al. (2002), Photochemical production of ozone in the upper troposphere in association with cumulus convection over Indonesia, *J. Geophys. Res.*, *107*(D3), 8400, doi:10.1029/2001JD000844, [printed 108(D3), 2003].

Kumar, R., M. Naja, G. G. Pfister, M. C. Barth, C. Wiedinmyer, and G. P. Brasseur (2012), Simulations over South Asia using the weather research and forecasting model with chemistry (WRF-Chem): Chemistry evaluation and initial results, *Geosci. Model Dev.*, *5*, 619–648.

Kunhikrishnan, T., M. G. Lawrence, R. von Kuhlmann, M. O. Wenig, A. H. Asman, A. Richter, and J. P. Burrows (2006), Regional NOx emission strength for the Indian subcontinent and the impact of emissions from India and neighboring countries on regional O3 chemistry, *J. Geophys. Res.*, *111*, D15301, doi:10.1029/2005JD006036.

Lal, S., L. K. Sahu, and S. Venkataramani (2007), Impact of transport from the surrounding continental regions on the distributions of ozone and related trace gases over the Bay of Bengal during February 2003, *J. Geophys. Res.*, *112*, D14302, doi:10.1029/2006JD008023.

Lal, S., L. K. Sahu, S. Venkataramani, T. A. Rajesh, and K. S. Modh (2008), Distributions of O3, CO and NMHCs over the rural sites in central India, *J. Atmos. Chem.*, *61*(1), 73–84.

Lal, S., S. Venkataramani, S. Srivastava, S. Gupta, C. Mallik, M. Naja, T. Sarangi, Y. B. Acharya, and X. Liu (2013), Transport effects on the vertical distribution of tropospheric ozone over the tropical marine regions surrounding India, *J. Geophys. Res. Atmos.*, *118*, 1513–1524, doi:10.1002/jgrd.50180.

Lamarque, J. F., et al. (2010), Historical (1850–2000) gridded anthropogenic and biomass burning emissions of reactive gases and aerosols: Methodology and application, *Atmos. Chem. Phys.*, *10*(15), 7017–7039.
Langmann, B., and A. Heil (2004), Release and dispersion of vegetation and peat fire emissions, *Atmos. Chem. Phys.*, *4*, 2145–2160.
Lawrence, M. G., and J. Lelieveld (2010), Atmospheric pollutant outflow from southern Asia: A review, *Atmos. Chem. Phys.*, *10*(22), 11,017–11,096, doi:10.5194/acp-10-11017-2010.
Lawrence, M. G., R. von Kuhlmann, M. Salzmann, and P. J. Rasch (2003), The balance of effects of deep convective mixing on tropospheric ozone, *Geophys. Res. Lett.*, *30*(18), 1940, doi:10.1029/2003GL017644.
Lelieveld, J., et al. (2001), The Indian Ocean Experiment: Widespread air pollution from South and Southeast Asia, *Science*, *291*(5506), 1031–1036.
Levelt, P. F., G. H. J. van den Oord, M. R. Dobber, A. Malkki, H. Visser, J. de Vries, P. Stammes, J. O. V. Lundell, and H. Saari (2006), The ozone monitoring instrument, *IEEE Trans. Geosci. Remote Sens.*, *44*, 1093–1101.
Logan, J. (1999), An analysis of ozonesonde data for the troposphere: Recommendations for testing 3-D models and development of a gridded climatology for tropospheric ozone, *J. Geophys. Res.*, *104*, 16,115–16,149, doi:10.1029/1998JD100096.
Mandal, T. K., D. Kley, H. G. J. Smit, S. K. Srivastava, S. K. Peshin, and A. P. Mitra (1999), Vertical distribution of ozone over the Indian Ocean (15°N–20°S) during First Field Phase INDOEX-1998, *Curr. Sci.*, *76*, 938–943.
Marenco, A., et al. (1998), Measurement of ozone and water vapor by Airbus in-service aircraft: The MOZAIC airborne program, An overview, *J. Geophys. Res.*, *103*, 25,631–25,642, doi:10.1029/98JD00977.
Monks, P. S., et al. (2009), Atmospheric composition change—Global and regional air quality, *Atmos. Environ.*, *43*, 5268–5350, doi:10.1016/j.atmosenv.2009.08.021.
Nassar, R., J. A. Logan, I. A. Megretskaia, L. T. Murray, L. Zhang, and D. B. A. Jones (2009), Analysis of tropical tropospheric ozone, carbon monoxide, and water vapor during the 2006 El Niño using TES observations and the GEOS-Chem model, *J. Geophys. Res.*, *114*, D17304, doi:10.1029/2009JD011760.
Nodzu, M. I., S.-Y. Ogino, Y. Tachibana, and M. D. Yamanaka (2006), Climatological description of seasonal variations in lower-tropospheric temperature inversion layers over the Indochina Peninsula, *J. Clim.*, *19*(13), 3307–3319.
Ohara, T., H. Akimoto, J. Kurokawa, N. Horii, K. Yamaji, X. Yan, and T. Hayasaka (2007), An Asian emission inventory of anthropogenic emission sources for the period 1980–2020, *Atmos. Chem. Phys. Discuss.*, *7*, 6843–6902, doi:10.5194/acpd-7-6843-2007.
Olivier, J. G. J., J. A. H. W. Peters, J. Bakker, J. J. M. Berdowski, A. J. H. Visschedijk, and J. P. J. Bloos (2002), Applications of EDGAR: Emission database for global atmospheric research, Rep. 410.200.051.RIVM, Rijksinst. voor Volkzgezondh. en Milieu, Bilthoven, Neth.
Oltmans, S. J., et al. (2006), Long-term changes in tropospheric ozone, *Atmos. Environ.*, *40*, 3156–3173, doi:10.1016/j.atmosenv.2006.01.029.
Onogi, K., et al. (2007), The JRA-25 Reanalysis, *J. Meteorol. Soc. Jpn.*, *85*, 369–432, doi:10.2151/jmsj.85.369.
Ordonez, C., et al (2010), Global model simulations of air pollution during the 2003 European heat wave, *Atmos. Chem. Phys.*, *10*(2), 789–815.
Park, M., W. J. Randel, A. Gettelman, S. T. Massie, and J. H. Jiang (2007), Transport above the Asian summer monsoon anticyclone inferred from Aura Microwave Limb Sounder tracers, *J. Geophys. Res.*, *112*, D16309, doi:10.1029/2006JD008294.
Paulik, L. C., and T. Birner (2012), Quantifying the deep convective temperature signal within the tropical tropopause layer (TTL), *Atmos. Chem. Phys.*, *12*, 12,183–12,195, doi:10.5194/acp-12-12183-2012.
Peshin, S. K., T. K. Mandal, H. G. J. Smit, S. K. Srivastav, and A. P. Mitra (2001), Observations of vertical distribution of tropospheric ozone over Indian Ocean and its comparison with continental profiles during INDOEX-FFP-1998 and IFP-1999, *Curr. Sci. (Suppl.)*, *80*, 197–208.
Pickering, K. E., A. M. Thompson, J. R. Scala, W. Tao, R. R. Dickerson, and J. Simpson (1992), Free tropospheric ozone production following entrainment of urban plumes into deep convection, *J. Geophys. Res.*, *97*, 17,985–18,000.
Prather, M., et al. (2001), Atmospheric chemistry and greenhouse gases, in *Climate Change 2001: The Scientific Basis*, Contribution of Working Group I to the Third Assessment Report of the Intergovernmental Panel on Climate Change, edited by J. T. Houghton et al., pp. 239–288, Cambridge Univ. Press, New York.
Reddy, B. S. K., L. S. S. Reddy, J.-J. Cao, K. R. Kumar, G. Balakrishnaiah, K. R. Gopal, R. R. Reddy, K. Narasimhulu, S. Lal, and Y. N. Ahammed (2011), Simultaneous measurements of surface ozone at two sites over the southern Asia: A comparative study, *Aerosol Air Qual. Res.*, *11*(7), 895–902, doi:10.4209/aaqr.2011.05.0061.
Sahu, L. K. (2012), Volatile organic compounds and their measurements in the troposphere, *Curr. Sci.*, *102*(10), 1645–1649.
Sahu, L. K., and S. Lal (2006), Changes in surface ozone levels due to convective downdrafts over the Bay of Bengal, *Geophys. Res. Lett.*, *33*, L10807, doi:10.1029/2006GL025994.
Sahu, L. K., and V. Sheel (2013), Spatio-temporal variation of biomass burning sources over South and Southeast Asia, *J. Atmos. Chem.*, doi:10.1007/s10874-013-9275-4, in press.
Sahu, L. K., S. Lal, and S. Venkataramani (2006), Distributions of O3, CO and hydrocarbons over the Bay of Bengal: A study to assess the role of transport from southern India and marine regions during September–October 2002, *Atmos. Environ.*, *40*, 4633–4645.
Sahu, L. K., S. Lal, V. Thouret, and H. G. Smit (2009a), Seasonality of tropospheric ozone and water vapor over Delhi, India: A study based on MOZAIC measurement data, *J. Atmos. Chem.*, *62*, 151–174, doi:10.1007/s10874-010-9146-1.
Sahu, L. K., Y. Kondo, Y. Miyazaki, M. Kuwata, M. Koike, N. Takegawa, H. Tanimoto, H. Matsueda, S. C. Yoon, and Y. J. Kim (2009b), Anthropogenic aerosols observed in Asian continental outflow at Jeju Island, Korea, in spring 2005, *J. Geophys. Res.*, *114*, D03301, doi:10.1029/2008JD010306.
Sahu, L. K., S. Lal, V. Thouret, and H. G. Smit (2010), Climatology of tropospheric ozone and water vapour over Chennai: A study based on MOZAIC measurements over India, *Int. J. Climatol.*, *31*, 920–936, doi:10.1002/joc.2128.
Sahu, L. K., Y. Kondo, Y. Miyazaki, P. Pongkiatkul, and N. T. Kim Oanh (2011), Seasonal and diurnal variations of black carbon and organic carbon aerosols in Bangkok, *J. Geophys. Res.*, *116*, D15302, doi:10.1029/2010JD015563.
Sahu, L. K., V. Sheel, M. Kajino, and P. Nedele (2013a), Variability in tropospheric carbon monoxide over an urban site in Southeast Asia, *Atmos. Environ.*, *68*, 243–255.
Sahu, L. K., V. Sheel, M. Kajino, S. S. Gunthe, V. Thouret, P. Nedelec, and H. G. Smit (2013b), Characteristics of tropospheric ozone variability over an urban site in Southeast Asia: A study based on MOZAIC and MOZART vertical profiles, *J. Geophys. Res. Atmos.*, *118*, 8729–8747, doi:10.1002/jgrd.50662.
Sauvage, B., V. Thouret, J.-P. Cammas, F. Gueusi, G. Athier, and P. Nédélec (2005), Tropospheric ozone over Equatorial Africa: Regional aspects from the MOZAIC data, *Atmos. Chem. Phys.*, *5*, 311–335.
Sauvage, B., R. V. Martin, A. van Donkelaar, and J. R. Ziemke (2007a), Quantification of the factors controlling tropical tropospheric ozone and the South Atlantic maximum, *J. Geophys. Res.*, *112*, D11309, doi:10.1029/2006JD008008.
Sauvage, B., R. V. Martin, A. van Donkelaar, X. Liu, K. Chance, L. Jaeglé, P. I. Palmer, S. Wu, and T.-M. Fu (2007b), Remote sensed and in situ constraints on processes affecting tropical tropospheric ozone, *Atmos. Chem. Phys.*, *7*(3), 815–838.

Sherwood, S. C., and A. E. Dessler (2003), Convective mixing near the tropical tropopause: Insights from seasonal variations, *J. Atmos. Sci.*, *60*, 2674–2685.
Shibata, K., M. Deushi, T. T. Sekiyama, and H. Yoshimura (2005), Development of an MRI chemical transport model for the study of stratospheric chemistry, *Pap. Meteorol. Geophys.*, *55*, 75–119.
Sinha, P. R., R. K. Manchanda, D. G. Kaskaoutis, Y. B. Kumar, and S. Sreenivasan (2013), Seasonal variation of surface and vertical profile of aerosol properties over a tropical urban station Hyderabad, India, *J. Geophys. Res. Atmos.*, *118*, 749–768, doi:10.1029/2012JD018039.
Srivastava, S., and V. Sheel (2012), Study of tropospheric CO and O3 enhancement episode over Indonesia during Autumn 2006 using the Model for Ozone and Related chemical Tracers (MOZART-4), *Atmos. Environ.*, *67*, 53–62.
Srivastava, S., S. Lal, S. Venkataramani, S. Gupta, and Y. B. Acharya (2011), Vertical distribution of ozone in the lower troposphere over the Bay of Bengal and the Arabian Sea during ICARB-2006: Effects of continental outflow, *J. Geophys. Res.*, *116*, D13301, doi:10.1029/2010JD015298.
Stevenson, D. S., et al. (2006), Multimodel ensemble simulations of present-day and near-future tropospheric ozone, *J. Geophys. Res.*, *111*, D08301, doi:10.1029/2005JD006338.
Streets, D. G., et al. (2003a), An inventory of gaseous and primary aerosol emissions in Asia in the year 2000, *J. Geophys. Res.*, *108*(D21), 8809, doi:10.1029/2002JD003093.
Streets, D. G., K. F. Yarber, J.-H. Woo, and G. R. Carmichael (2003b), Biomass burning in Asia: Annual and seasonal estimates and atmospheric emissions, *Global Biogeochem. Cycles*, *17*(4), 1099, doi:10.1029/2003GB002040.
Swamy, Y. V., R. Venkanna, G. N. Nikhil, D. N. S. K. Chitanya, P. R. Sinha, M. Ramakrishna, and A. G. Rao (2012), Impact of nitrogen oxides, volatile organic compounds and black Carbon on atmospheric ozone levels at a semi arid urban site in Hyderabad, *Aerosol Air Qual. Res.*, *12*, 662–671.
Thompson, A. M., J. C. Witte, R. D. Hudson, H. Guo, J. R. Herman, and M. Fujiwara (2001), Tropical tropospheric ozone and biomass burning, *Science*, *291*, 2128–2132.
Thompson, A. M., et al. (2003), Southern Hemisphere Additional Ozonesondes (SHADOZ) 1998–2000 tropical ozone climatology: 1. Comparison with Total Ozone Mapping Spectrometer (TOMS) and ground-based measurements, *J. Geophys. Res.*, *108*(D2), 8238, doi:10.1029/2001JD000967.
Thouret, V., A. Marenco, P. Nédélec, and C. Grouhel (1998a), Ozone climatologies at 9–12 km altitude as seen by the MOZAIC airborne program between September 1994 and August 1996, *J. Geophys. Res.*, *103*, 25,653–25,680.
Thouret, V., A. Marenco, J. A. Logan, P. Nédélec, and C. Grouhel (1998b), Comparisons of ozone measurements from the MOZAIC airborne program and the ozone sounding network at eight locations, *J. Geophys. Res.*, *103*, 25,695–25,720.
van der Werf, G. R., J. T. Randerson, L. Giglio, G. J. Collatz, P. S. Kasibhatla, and A. F. Arellano (2006), Interannual variability of global biomass burning emissions from 1997 to 2004, *Atmos. Chem. Phys.*, *6*, 3423–3441, doi:10.5194/acp-6-3423-2006.
van der Werf, G. R., J. T. Randerson, L. Giglio, G. J. Collatz, M. Mu, P. S. Kasibhatla, D. C. Morton, R. S. DeFries, Y. Jin, and T. T. van Leeuwen (2010), Global fire emissions and the contribution of deforestation, savanna, forest, agricultural, and peat fires (1997–2009), *Atmos. Chem. Phys.*, *10*, 11,707–11,735, doi:10.5194/acp-10-11707-2010.
Verma, R. L., et al. (2010), Temporal variations of black carbon in Guangzhou, China, in summer 2006, *Atmos. Chem. Phys.*, *10*, 6471–6485, doi:10.5194/acp-10-6471-2010.
Wang, X., and D. L. Mauzerall (2004), Characterizing distributions of surface ozone and its impact on grain production in China, Japan, and South Korea, *Atmos. Environ.*, *38*, 4383–4402.
Waters, J. W., et al. (2006), The Earth Observing System Microwave Limb Sounder (EOS MLS) on the Aura satellite, *IEEE Trans. Geosci. Remote Sens.*, *44*(5), 1075–1092.
Wong, M. L. M., and J. C. L. Chan (2004), Tropical cyclone intensity in vertical wind shear, *J. Atmos. Sci.*, *61*, 1859–1876.
Yonemura, S., H. Tsuruta, S. Kawashima, S. Sudo, L. C. Peng, L. S. Fook, Z. Johar, and M. Hayashi (2002), Tropospheric ozone climatology over Peninsular Malaysia from 1992 to 1999, *J. Geophys. Res.*, *107*(D15), 4229, doi:10.1029/2001JD000993.
Yoshimura, H., and S. Yukimoto (2008), Development of a Simple Coupler (Scup) for Earth System Modeling, *Pap. Meteorol. Geophys.*, *59*, 19–29.
Yukimoto, S., et al. (2011), Meteorological Research Institute Earth System Model Version 1 (MRI-ESM1)—Model Description—. Tech. Rep. of MRI, 64, 83 pp.
Yurganov, L. N., W. W. McMillan, A. V. Dzhola, E. I. Grechko, N. B. Jones, and G. R. van der Werf (2008), Global AIRS and MOPITT CO measurements: Validation, comparison, and links to biomass burning variations and carbon cycle, *J. Geophys. Res.*, *113*, D09301, doi:10.1029/2007JD009229.
Zachariasse, M., P. F. J. van Velthoven, H. G. J. Smit, J. Lelieveld, T. K. Mandal, and H. Kelder (2000), Influence of stratosphere-troposphere exchange on tropospheric ozone over the tropical Indian Ocean during the winter monsoon, *J. Geophys. Res.*, *105*, 15,403–15,416.
Zhang, L., Q. B. Li, J. Jin, H. Liu, N. Livesey, J. H. Jiang, Y. Mao, D. Chen, M. Luo, and Y. Chen (2011), Impacts of 2006 Indonesian fires and dynamics on tropical upper tropospheric carbon monoxide and ozone, *Atmos. Chem. Phys.*, *11*(21), 10,929–10,946.
Ziemke, J. R., and S. Chandra (2003), La Nina and El Nino-induced variabilities of ozone in the tropical lower atmosphere during 1970–2001, *Geophys. Res. Lett.*, *30* (3), 1142, doi:10.1029/2002GL016387.
Ziemke, J. R., S. Chandra, M. R. Schoeberl, L. Froidevaux, W. G. Read, P. F. Levelt, and P. K. Bhartia (2007), Intra-seasonal variability in tropospheric ozone and water vapor in the tropics, *Geophys. Res. Lett.*, *34*, L17804, doi:10.1029/2007GL030965.